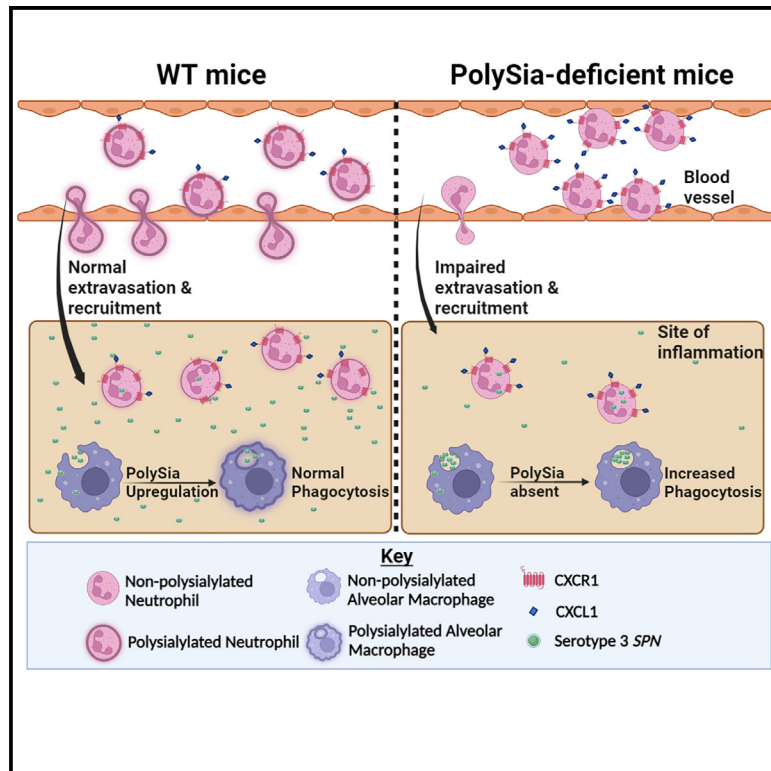


## Polysialylation controls immune function of myeloid cells in murine model of pneumococcal pneumonia

### Graphical abstract



### Authors

Prajakta Shinde, Alexander Kiepas, Lei Zhang, Shreya Sudhir, Konstantinos Konstantopoulos, Nicholas M. Stamatou

### Correspondence

nstamatou@ihv.umaryland.edu

### In brief

Comparing cells from ST8SialIV<sup>-/-</sup> and wild-type mice, Shinde et al. show the impact of progressive loss of polysialic acid from the surface of myeloid cells on cell migration and phagocytosis after infection with *Streptococcus pneumoniae*. They demonstrate the importance of tightly regulated expression of this glycan on individual cell types.

### Highlights

- PolySia is downregulated in myeloid cells during recruitment to *Spn* site of infection
- Overall polySia deficiency provides a survival advantage to *Spn*-infected mice
- Absence of polySia on alveolar macrophages promotes phagocytosis of encapsulated *Spn*
- ST8SialIV<sup>-/-</sup> neutrophils exhibit excess CXCL1 binding and ERK phosphorylation



## Article

# Polysialylation controls immune function of myeloid cells in murine model of pneumococcal pneumonia

Prajakta Shinde,<sup>1</sup> Alexander Kiepas,<sup>2</sup> Lei Zhang,<sup>1</sup> Shreya Sudhir,<sup>1</sup> Konstantinos Konstantopoulos,<sup>2</sup> and Nicholas M. Stamatos<sup>1,3,\*</sup><sup>1</sup>Institute of Human Virology, University of Maryland School of Medicine, Baltimore, MD 21201, USA<sup>2</sup>Department of Chemical and Biomolecular Engineering, Whiting School of Engineering, Johns Hopkins University, Baltimore, MD 21218, USA<sup>3</sup>Lead contact\*Correspondence: [nstamatos@ihv.umaryland.edu](mailto:nstamatos@ihv.umaryland.edu)<https://doi.org/10.1016/j.celrep.2023.112648>

## SUMMARY

Polysialic acid (polySia) is a post-translational modification of a select group of cell-surface proteins that guides cellular interactions. As the overall impact of changes in expression of this glycan on leukocytes during infection is not known, we evaluate the immune response of polySia-deficient ST8SialV<sup>-/-</sup> mice infected with *Streptococcus pneumoniae* (*Spn*). Compared with wild-type (WT) mice, ST8SialV<sup>-/-</sup> mice are less susceptible to infection and clear *Spn* from airways faster, with alveolar macrophages demonstrating greater viability and phagocytic activity. Leukocyte pulmonary recruitment, paradoxically, is diminished in infected ST8SialV<sup>-/-</sup> mice, corroborated by adoptive cell transfer, microfluidic migration experiments, and intravital microscopy, and possibly explained by dysregulated ERK1/2 signaling. PolySia is progressively lost from neutrophils and monocytes migrating from bone marrow to alveoli in *Spn*-infected WT mice, consistent with changing cellular functions. These data highlight multidimensional effects of polySia on leukocytes during an immune response and suggest therapeutic interventions for optimizing immunity.

## INTRODUCTION

*Streptococcus pneumoniae* (*Spn*) has historically been considered the most common etiology of community-acquired pneumonia worldwide.<sup>1</sup> Although effective *Spn* vaccines are available, the inherent virulence of this pathogen and increasing antibiotic resistance make *Spn* a leading cause of morbidity and mortality. Glycosylation plays a major role in the pathogenicity of *Spn*. A polysaccharide capsule protects *Spn* from phagocytosis, and *Spn*-encoded neuraminidase NanA has the potential to desialylate glycans on host cells.<sup>2</sup> A better understanding of how glycosylation of leukocytes is regulated during the host immune response to this pathogen is needed to improve therapeutic and preventive strategies.

Glycosylation of cell-surface proteins and lipids profoundly influences cellular interactions with ligands, microbes, and neighboring cells and helps direct cellular migration. By virtue of its terminal location on glycans and negative charge, sialic acid plays a vital role in regulating these diverse cellular activities that are essential for immunity. This nine-carbon sugar is commonly expressed in eukaryotic cells as a monomer that is  $\alpha$ 2-3 and  $\alpha$ 2-6 linked to the penultimate galactose of complex glycans. In contrast, polysialic acid (polySia), a unique hydrophilic and electronegative glycan composed of long chains of  $\alpha$ 2-8-linked monomeric sialic acid with a degree of polymerization greater

than seven residues, has been identified as a post-translational modification on only nine mammalian proteins.<sup>3–11</sup> Studied extensively in the developing central nervous system as a post-translational modification of the neural cell adhesion molecule (NCAM) that is involved in cell migration, axonal guidance, synapse formation, and functional plasticity,<sup>12,13</sup> polySia has only recently been shown to influence the function of cells of the immune system.<sup>14</sup>

We were among the first groups to demonstrate that polySia is expressed on the surface of myeloid cells and identified neuropilin 2 (NRP-2) as a carrier of polySia in primary human and mouse dendritic cells (DCs).<sup>4,15,16</sup> Subsequently, CCR7 and ESL-1 were also shown to carry polySia respectively, in human DCs and macrophages,<sup>7,9</sup> and NCAM/CD56 was found to be a carrier in mouse myeloid cells.<sup>17</sup> Based on the dynamic regulation of polySia expression during activation, migration, and differentiation of monocytes and neutrophils,<sup>16</sup> we proposed that the temporospatial-specific expression of this unique glycan on these cells is designed to support specific functions during an evolving immune response. In support of this concept, several roles for polySia on leukocytes have been reported and include (1) regulating the interaction of DCs with T lymphocytes,<sup>4</sup> (2) promoting DC migration by modulating CCR7 receptor recognition of chemokine CCL21,<sup>7,18–20</sup> (3) dampening activation of microglia by engaging SIGLECs,<sup>21,22</sup> and (4) controlling



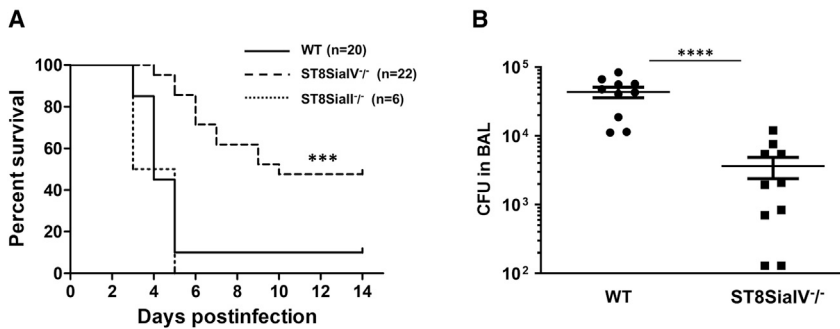


**Figure 1. ST8SialIV<sup>-/-</sup> mice are relatively resistant to pulmonary infection with *Spn* and clear the pathogen more effectively than WT mice**

(A and B) Eight- to 12-week-old WT, ST8SialIV<sup>-/-</sup>, and ST8SialII<sup>+/+</sup> mice were infected intratracheally with 10<sup>4</sup> colony-forming units (CFU) of *Spn* and were monitored daily for clinical signs of moribundity as described in STAR Methods (A). Pulmonary clearance of *Spn* was evaluated by quantitating CFU of *Spn* in the BAL fluid 24 h postinfection (B). Statistical significance of data from survival experiments in (A) was determined by log-rank test, and data in (B) are expressed as mean ± SEM (n = 3 mice per group) from each of four experiments. \*\*\*p ≤ 0.001; \*\*\*\*p ≤ 0.0001 (two-tailed t test).

phagocytosis of *Klebsiella pneumoniae* in peritoneal macrophages.<sup>16</sup> PolySia has also been reported to be expressed on activated human lymphocytes<sup>23</sup> with a proposed role in cell migration.<sup>24</sup>

Although the combined impact of changing expression of polySia on monocytes, neutrophils, and other cell types during systemic infection has yet to be reported, studies in mice have demonstrated the clinical relevance of polySia in immunity. Polysialyltransferase IV knockout (ST8SialIV<sup>-/-</sup>) mice<sup>25</sup> that lack polySia in immune cells<sup>17,24</sup> showed exaggerated contact hypersensitivity and an impaired capacity to control tumor growth compared with wild-type (WT) mice.<sup>17</sup> In separate studies, DC migration to draining lymph nodes in response to local lipopolysaccharide (LPS) injection was impaired in ST8SialIV<sup>-/-</sup> mice.<sup>7</sup> Understanding the role of polySia during an immune response also requires an appreciation of non-circulating cells such as lung epithelium, which can influence pulmonary immunity by secreting a soluble form of polysialylated NCAM/CD56.<sup>26</sup>

The innate immune response against bacterial respiratory pathogens depends on neutrophil and monocyte recruitment to the lung and on resident alveolar macrophages (AMs), and ideally involves effective pathogen clearance with limited tissue damage. We have shown that the amount of polySia on the surface of murine monocytes and neutrophils is reduced as they migrate from the bone marrow (BM) into peripheral blood (PB) during homeostatic conditions and is diminished below the level of detection when these cells reach the lungs in response to intratracheal LPS instillation.<sup>16</sup> Thus, it remains to be determined how progressive loss of polySia can be reconciled with its demonstrated importance for chemokine binding and migration of DCs.<sup>7,18,20</sup> We have also shown that removal of polySia from the surface of macrophages enhances phagocytosis of *K. pneumoniae*.<sup>16</sup> Thus, a mouse model of bacterial pneumonia is expected to provide a useful system to determine whether the enhanced phagocytosis resulting from removal of this glycan overshadows a possible dampening of cell recruitment to the site of infection. It will also help us to understand the combined effect of polysialylation of various cell types on immunity and dissect and possibly provide the basis for modifying the extent of polysialylation on these cell types to optimize the immune response.

In this report, we demonstrate that ST8SialIV<sup>-/-</sup> mice are less susceptible than WT mice to *Spn* infection. Although neutrophil and monocyte recruitment to the lungs of ST8SialIV<sup>-/-</sup> mice was diminished with less inflammatory tissue damage compared with WT mice, enhanced viability and phagocytic activity of AMs from ST8SialIV<sup>-/-</sup> mice led to early effective clearance of the pathogen. Adoptive transfer experiments and microfluidic chamber and transwell migration assays with BM neutrophils and monocytes from ST8SialIV<sup>-/-</sup> and WT mice confirmed the more robust migration of polysialylated cells in response to chemokine that was not explained by differences in chemokine receptor CXCR2 cell-surface density or in amount of bound chemokine in the case of neutrophils. Neither was it explained by enhanced intracellular signaling in response to chemoattractant, as neutrophils from ST8SialIV<sup>-/-</sup> mice revealed greater extracellular signal-regulated kinase ERK1/2 phosphorylation in response to *N*-formylmethionyl-leucyl-phenylalanine (fMLP) compared with WT neutrophils. In contrast to the migration advantage conferred by polySia, the absence of polySia led to tighter adhesion of neutrophils from ST8SialIV<sup>-/-</sup> mice to vascular endothelium and impaired extravasation, as demonstrated by intravital microscopy. The dynamic downregulation of polySia expression from the surface of neutrophils and monocytes as they migrate from the BM in response to *Spn* lung infection appears to be designed to optimize cell function at particular steps of the immune response. Our results demonstrate that despite the importance of cellular polySia for some aspects of immune cell activity, there is an overall host-protective advantage of polySia deficiency in murine bacterial pulmonary infection.

## RESULTS

### ST8SialIV<sup>-/-</sup> mice are relatively resistant to *Streptococcus pneumoniae* infection

To determine the relative importance of host polySia during pulmonary infection with *Spn*, survival of ST8SialIV<sup>-/-</sup> mice was compared with that of WT mice after each was infected with a lethal dose of *Spn*. When WT mice were infected intratracheally (i.t.) with 1 × 10<sup>4</sup> colony-forming units (CFU) of *Spn*, >90% of mice revealed moribundity 5 days postinfection (Figure 1A). In contrast, ST8SialIV<sup>-/-</sup> mice, which are devoid of detectable

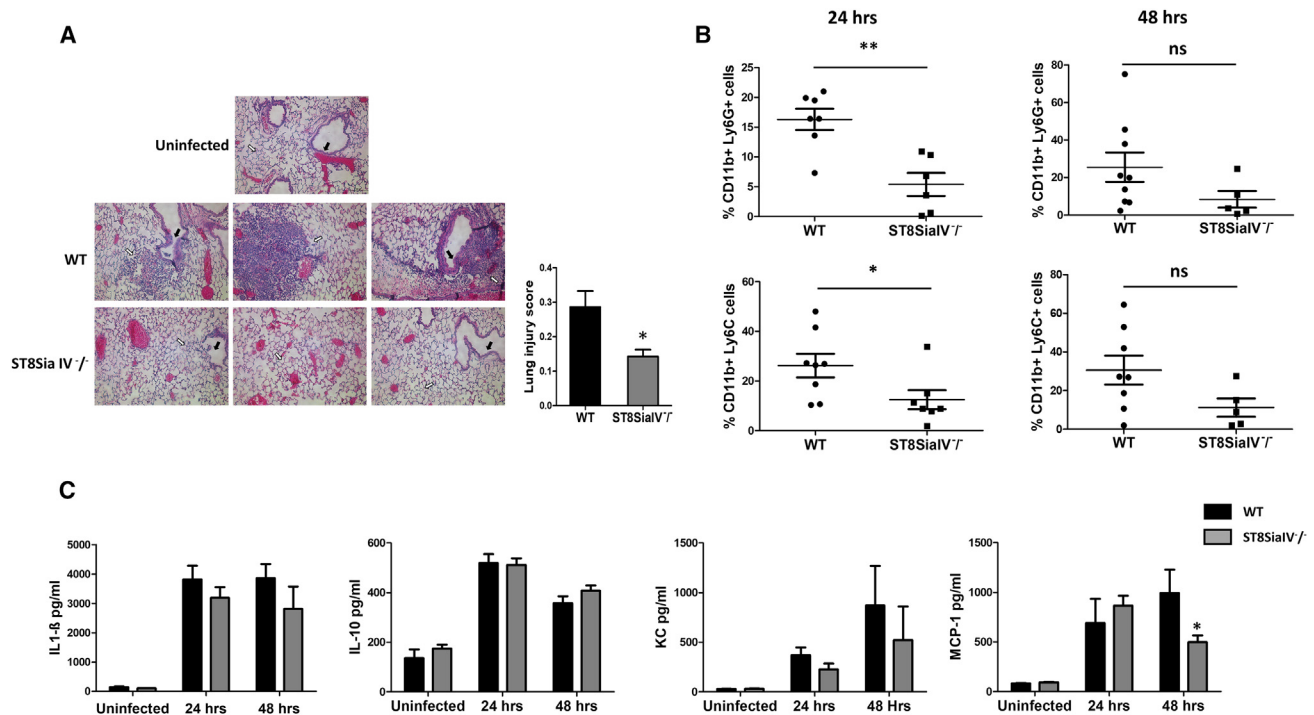


**Figure 2. Pulmonary recruitment of myeloid cells from ST8SialIV<sup>-/-</sup> mice is impaired following infection with *Spn***

(A) Lung sections from uninfected and *Spn*-infected WT and ST8SialIV<sup>-/-</sup> mice 24 h postinfection were stained with H&E and imaged at 10× magnification, and lung injury score was determined as described in STAR Methods (white arrowheads indicate alveolar spaces; black arrowheads indicate bronchial walls). (B) Leukocytes were harvested from BAL fluid from WT and ST8SialIV<sup>-/-</sup> mice 24 h and 48 h postinfection with *Spn* and were analyzed by flow cytometry after staining with antibodies to CD45, CD11b, Ly6C, and Ly6G, and the percentage of neutrophils (CD11b, Ly6G; upper panels) and monocytes (CD11b, Ly6C; lower panels) in CD45 gated cells was determined (for gating strategy see Figure S2). (C) Lung homogenates from uninfected WT and ST8SialIV<sup>-/-</sup> mice and from mice 24 h and 48 h postinfection with *Spn* were prepared, and levels of IL-1β (left), IL-10 (second from left), KC (second from right), and MCP-1 (right) were measured by ELISA; WT (black bars), and ST8SialIV<sup>-/-</sup> (gray bars). Data in (B) and (C) represent values from individual mice from five independent experiments and were evaluated by t test with mean ± SEM. \*p ≤ 0.05; \*\*p ≤ 0.01; ns, not statistically significant. Scale bars, 100 μm.

polySia in leukocytes (Figure S1)<sup>7,17</sup> and revealed no difference with WT mice in terms of relative numbers of CD45-gated myeloid subsets in BM and PB (Figure S2),<sup>17,24</sup> showed delayed morbidity, with only 50% of mice showing severe illness up to 14 days postinfection (p ≤ 0.001). Polysialyltransferase II knockout (ST8SialII<sup>-/-</sup>) mice, which are also deficient in polySia but display no detectable deficits in leukocyte polySia expression,<sup>17</sup> showed progression of *Spn* infection, similar to WT mice. Consistent with the difference in survival between the two strains of mice, there was a significantly lower burden of *Spn* in the bronchoalveolar lavage (BAL) fluid of ST8SialIV<sup>-/-</sup> (3,646 ± 1,247 CFU) compared with WT (43,640 ± 7,608 CFU) mice 24 h postinfection (Figure 1B). These results suggest that the absence of polySia on cells of the immune system enhances clearance of the bacterial pathogen, thus providing a potential explanation for the greater survival of ST8SialIV<sup>-/-</sup> mice.

### Pulmonary recruitment of ST8SialIV<sup>-/-</sup> myeloid cells is compromised in *Spn* infection

As it has previously been shown that polySia affects DC migration,<sup>7,18,19</sup> we determined whether a potential difference in immune cell recruitment to the lungs of WT and ST8SialIV<sup>-/-</sup>

mice postinfection might partly explain the differences in survival and bacterial clearance of these two mouse strains. Lung sections from *Spn*-infected WT mice had more pronounced cellular infiltrates than did lung tissue from *Spn*-infected ST8SialIV<sup>-/-</sup> mice as early as 24 h postinfection (Figure 2A). There were numerous patchy parenchymal infiltrates in alveolar spaces (white arrows) and thick bronchial walls (black arrows) in lungs of infected WT mice (Figure 2A, middle row). In contrast, the lungs of infected ST8SialIV<sup>-/-</sup> mice appeared similar to those of uninfected mice (Figure 2A, lower and top rows, respectively). These findings were reflected in a lung injury score for WT mice that was significantly greater than that for ST8SialIV<sup>-/-</sup> mice (0.2860 ± 0.0466 versus 0.1420 ± 0.0206; p = 0.0301) (Figure 2A). These histological results were confirmed by flow cytometry, which revealed significantly more total neutrophils (CD11b<sup>+</sup>, Ly6G<sup>+</sup>) and monocytes (CD11b<sup>+</sup>, Ly6C<sup>+</sup>) in CD45-gated leukocytes in the BAL fluid of *Spn*-infected WT compared with ST8SialIV<sup>-/-</sup> mice 24 h postinfection, with that difference persisting after 48 h (Figure 2B). That the difference in cell migration was not related to different levels of relevant chemokines was shown by equivalent amounts of CXCL1/keratinocyte-derived factor (KC), MCP-1, interleukin-10 (IL-10), and IL-1β recovered from

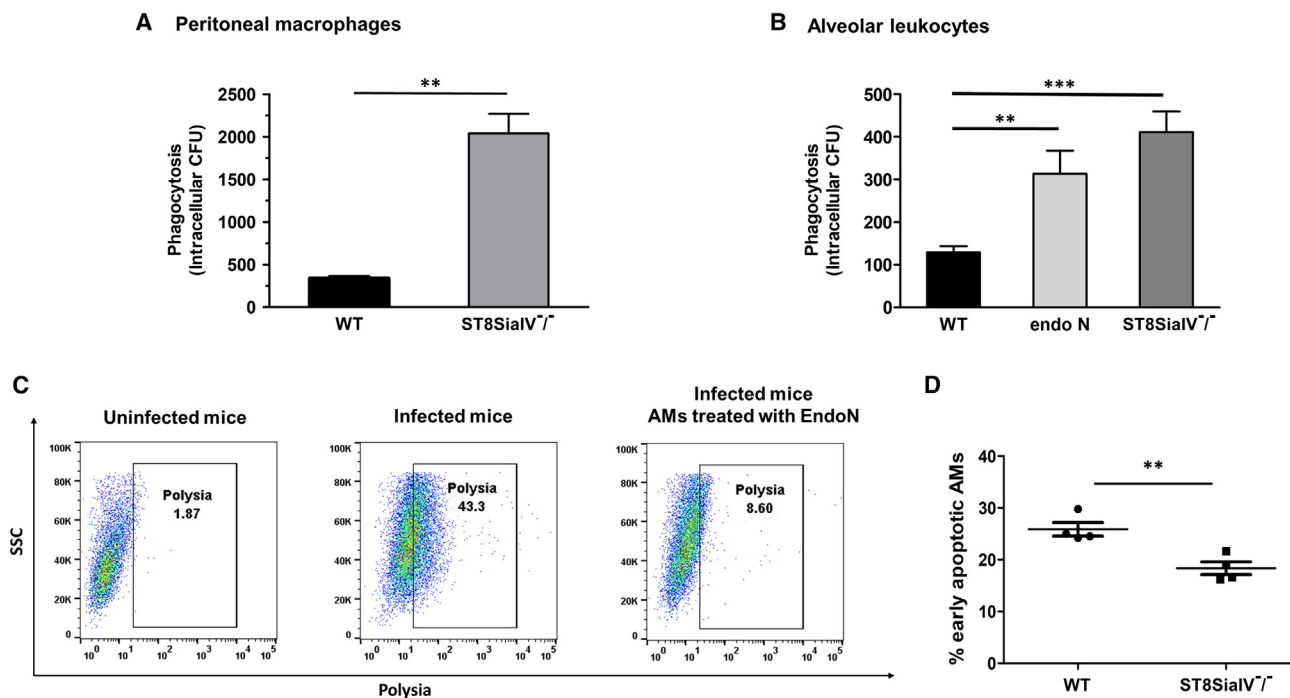


**Figure 3. Absence of polySia in leukocytes from *ST8SialV*<sup>-/-</sup> mice promotes phagocytosis of *Spn***

(A) Peritoneal macrophages were isolated from WT and *ST8SialV*<sup>-/-</sup> mice, grown in tissue culture plates for 24 h, incubated with opsonized *Spn*, and lysed to quantitate the number of intracellular bacteria (CFU) as described in STAR Methods.

(B) Leukocytes from WT mice (with or without treatment with endoN) and from *ST8SialV*<sup>-/-</sup> mice were collected by BAL, incubated with opsonized *Spn*, and lysed to quantitate intracellular CFU as described in STAR Methods.

(C) Cells that were collected by BAL from uninfected WT mice and from WT mice 24 h postinfection with *Spn* (with or without endoN treatment) were stained with antibody against CD45, CD11b, CD11c, Ly6C, Siglec F, and polySia, and polySia expression on gated AMs (CD11c<sup>+</sup>, Siglec F<sup>+</sup>) is shown in the dot plots. SSC, side scatter.

(D) Cells that were collected by BAL from uninfected WT mice were stained with antibody against CD45, CD11c, and Siglec F and with annexin V and 7-AAD, and the percentage of AMs displaying early apoptosis was analyzed by flow cytometry.

Data in (A), (B), and (D) are expressed as mean ± SEM of each assay using cells from three mice per group from each of three experiments. \*\*p ≤ 0.01; \*\*\*p ≤ 0.001 (two-tailed t test). Data in (C) are representative of three different experiments.

total lung homogenates of infected WT and *ST8SialV*<sup>-/-</sup> mice 24 h postinfection (Figure 2C), despite the altered lung pathology. These data raise an interesting paradox in that greater survival and bacterial clearance are associated with a muted immune cell infiltration in *ST8SialV*<sup>-/-</sup> mice.

### Phagocytic cells from *ST8SialV*<sup>-/-</sup> mice clear *Spn* more effectively than WT cells during early immune response

The survival advantage of *ST8SialV*<sup>-/-</sup> mice could potentially be attributable to several factors such as less severe tissue damage as a result of muted immune cell infiltration and enhanced clearance of *Spn* by more efficient phagocytosis. We previously reported that the loss of polySia from the surface of peritoneal macrophages enhanced the phagocytosis of gram-negative *K. pneumoniae*.<sup>16</sup> As thioglycolate-induced peritoneal macrophages are more abundant than AMs, we first determined whether cell-surface polySia also affects phagocytosis of encapsulated, gram-positive *Spn* using peritoneal macrophages from *ST8SialV*<sup>-/-</sup> and WT mice. As expected from our earlier studies, peritoneal macrophages from *ST8SialV*<sup>-/-</sup> mice phagocytosed opsonized *Spn* more effectively than did WT peritoneal macro-

phages (Figure 3A). To determine whether cell-surface polySia also affects phagocytosis of *Spn* by AMs and other alveolar leukocytes, mice received an i.t. instillation of LPS 20 h prior to cell harvest to obtain sufficient cells to conduct the phagocytosis assay. Similar to results with peritoneal macrophages, alveolar leukocytes from *ST8SialV*<sup>-/-</sup> mice phagocytosed opsonized *Spn* more efficiently than did cells from WT mice (Figure 3B). Removal of polySia from the surface of WT BAL leukocytes using endoglycosidase N (endoN), an enzyme that specifically cleaves chains of polySia,<sup>27,28</sup> also enhanced phagocytosis of *Spn*, albeit to a lesser extent than did cells from *ST8SialV*<sup>-/-</sup> mice (Figure 3B). It should be noted that although AMs from uninfected WT mice under homeostatic conditions are devoid of detectable cell-surface polySia, expression of this glycan on the cell surface is upregulated within 24 h after infection with *Spn* (Figure 3C), a time when there are equivalent numbers of AMs in WT and *ST8SialV*<sup>-/-</sup> mice (Figure S3). To complement the enhanced phagocytosis of *Spn* by BAL leukocytes from *ST8SialV*<sup>-/-</sup> mice, the viability of AMs from these mice was also greater than that of AMs from WT mice when evaluated 24 h postinfection (Figure 3D). Thus, enhanced phagocytosis of *Spn* and delayed apoptosis of AMs from

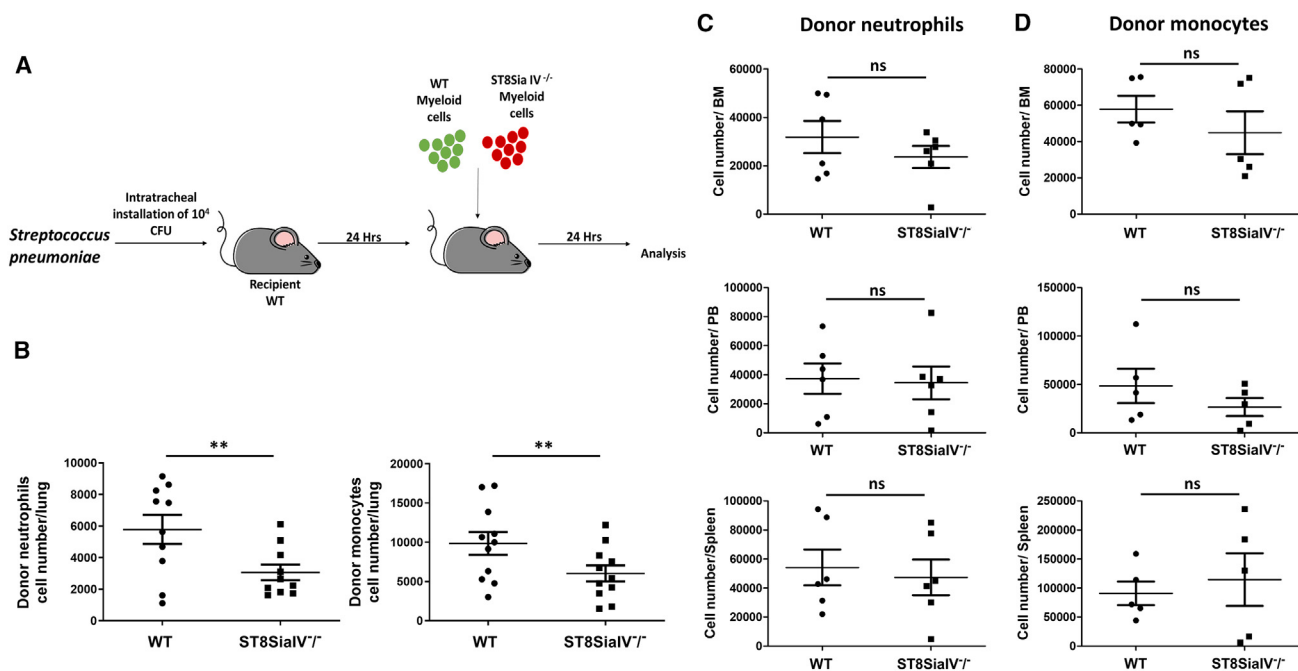


**Figure 4. Adoptively transferred neutrophils and monocytes from ST8SialIV<sup>-/-</sup> mice migrate less efficiently than WT cells to lungs of recipient *Spn*-infected WT mice**

(A) Schematic representation of adoptive transfer experiment performed on *Spn*-infected WT mice. (B) Total lung was harvested from *Spn*-infected WT mice 24 h after receiving an intra-orbital injection of differentially labeled WT and ST8SialIV<sup>-/-</sup> BM-derived neutrophils or monocytes, and the number of labeled donor neutrophils (left) and monocytes (right) was determined by flow cytometry. (C and D) Cells from BM, PB, and spleen of adoptively transferred mice were harvested, and the number of labeled donor neutrophils (C) and donor monocytes (D) was determined by flow cytometry. Data in (B), (C), and (D) are expressed as mean ± SEM (n = 2–3 mice per group) from each of four experiments. \*\*p ≤ 0.01; ns, not significant (non-parametric Wilcoxon signed-rank test).

ST8SialIV<sup>-/-</sup> mice are possible explanations for the greater capacity to clear *Spn* at early times postinfection.

### Polysialic acid expressed in neutrophils and monocytes promotes homing to pulmonary site of infection

To establish whether the reduced pulmonary recruitment of leukocytes in ST8SialIV<sup>-/-</sup> mice during infection with *Spn* is related to an absence of polySia specifically on neutrophils and monocytes, these cells from WT and ST8SialIV<sup>-/-</sup> mice were adoptively transferred into WT mice and their localization to the lungs was compared. When CFDA-SE-labeled WT and Deep Red-labeled ST8SialIV<sup>-/-</sup> BM neutrophils or monocytes were intra-orbitally injected into the same WT recipient mouse 24 h after infection with *Spn*, labeled donor cells were detected after an additional 24 h in BM, PB, spleen, and lungs (Figures 4A–4D). Whereas a similar number of labeled donor neutrophils and monocytes from both mouse strains was detected in BM, PB, and spleen of recipient mice (Figures 4C and 4D), a significantly greater number of WT donor neutrophils and monocytes compared with cells from ST8SialIV<sup>-/-</sup> donor mice was present in the total lung homogenate of recipients (Figure 4B). These *in vivo* experiments demonstrate that polySia expression on neutrophils and monocytes governs their migration and recruitment to the pulmonary site of infection.

To corroborate these results, microfluidic chamber and transwell migration assays were performed to evaluate migration *in vitro* of BM leukocytes toward a specific chemoattractant. When neutrophil migration was evaluated in microfluidic chambers, WT neutrophils demonstrated significantly greater speed, velocity, and persistence toward both fMLP and CXCL1/KC chemokine gradients compared with neutrophils from ST8SialIV<sup>-/-</sup> mice (Figures 5A and 5B). In addition, a greater number of purified BM neutrophils from WT mice migrated toward KC into the lower chamber of a transwell plate compared with ST8SialIV<sup>-/-</sup> neutrophils (Figure S4A). The more robust migration of WT neutrophils was not a result of differential expression of the KC receptor CXCR1, as equivalent amounts of the receptor were detected on the surface of neutrophils from WT and ST8SialIV<sup>-/-</sup> mice (Figure 5C). Neither was the enhanced migration of WT neutrophils a result of greater affinity of KC to polysialylated cells, as KC bound preferentially to ST8SialIV<sup>-/-</sup> neutrophils compared with WT cells (Figure 5D), nor of enhanced mitogen-activated protein kinase signaling, as phosphorylation of ERK1/2 in ST8SialIV<sup>-/-</sup> neutrophils was on average at least 1.6-fold more robust than in WT cells 2.5 and 5 min after exposure to fMLP (Figure 5E). As seen with neutrophils, purified BM monocytes from WT mice migrated more effectively

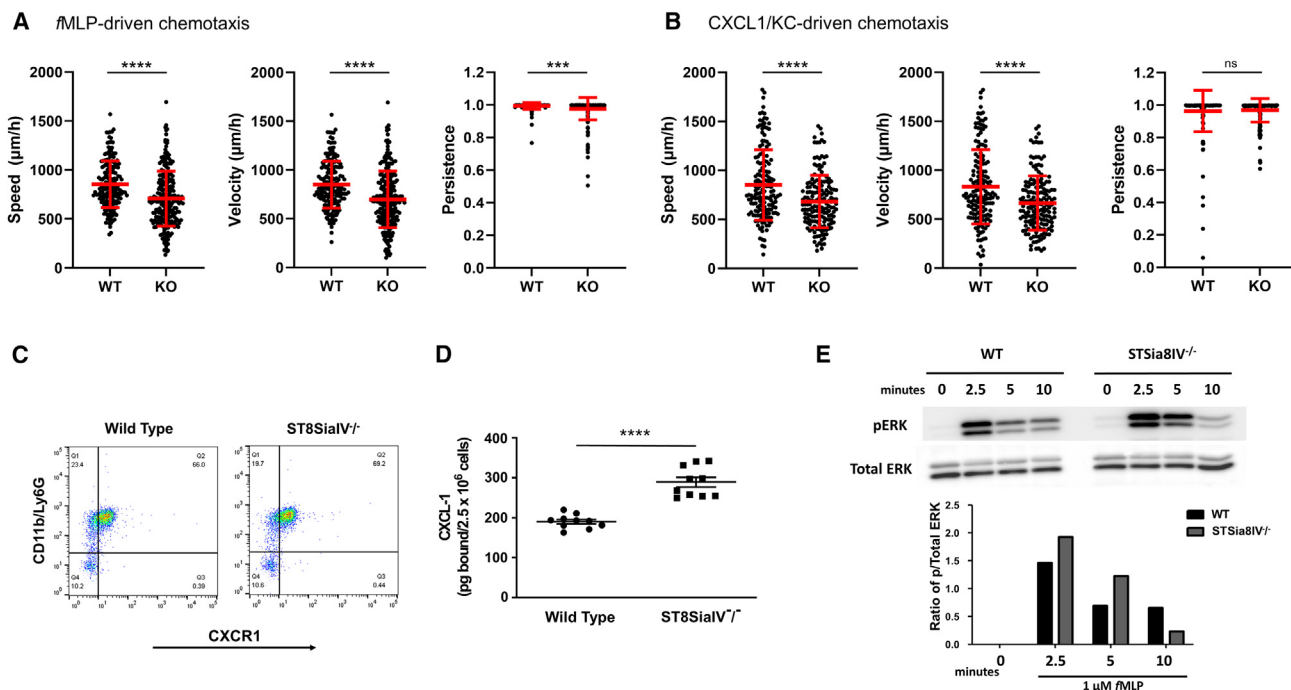


**Figure 5. Migration *in vitro* of ST8SialIV<sup>-/-</sup> neutrophils toward CXCL1 and fMLP is compromised compared with WT neutrophils**

(A and B) Chemotaxis of neutrophils from WT and ST8SialIV<sup>-/-</sup> mice was evaluated in a microfluidic-based microchannel assay, as described in STAR Methods. Cell migration toward fMLP (A) and CXCL1/KC (B) gradients was visualized and recorded by time-lapse live microscopy. The speed, velocity, and persistence of cells was computed from individual cell tracks ( $n = 191$  and  $n = 234$  from WT and ST8SialIV<sup>-/-</sup> mice, respectively). Data are expressed as mean  $\pm$  SD using cells from three mice per group from each of four experiments. \*\*\* $p \leq 0.001$ ; \*\*\*\* $p \leq 0.0001$ ; ns, not significant (Welch's t test).

(C) Bone marrow neutrophils from WT and ST8SialIV<sup>-/-</sup> mice were isolated and stained for CD11b, Ly6G and CXCR1 and were analyzed by flow cytometry. Dot plots represent data from five mice of each strain.

(D) Bone marrow neutrophils were isolated and incubated with CXCL1/KC (100 ng/mL), washed five times with PBS, lysed in RIPA buffer, and analyzed for bound CXCL1/KC by ELISA. Data are expressed as mean  $\pm$  SEM ( $n = 3$  mice per group) from each of three experiments. \*\*\*\* $p \leq 0.0001$  (two-tailed t test).

(E) Bone marrow neutrophils were isolated and incubated with 1  $\mu$ M fMLP for the indicated times and collected and lysed in RIPA buffer, and equal amounts of protein (25  $\mu$ g) from each lysate was separated on SDS-PAGE and analyzed for the amount of phosphorylated and total ERK as indicated in STAR Methods. Histogram shows the ratio of phosphorylated to total ERK at each time point. The immunoblot is representative of results obtained from three independent experiments.

toward chemokine CCL2 in a transwell migration assay compared with ST8SialIV<sup>-/-</sup> and endoN-treated BM monocytes (Figure S4B).

The effect of surface polySia on leukocyte migration *in vivo* was evaluated further using intravital microscopy. When labeled WT and ST8SialIV<sup>-/-</sup> BM neutrophils were adoptively transferred into WT mice and visualized circulating through the cremasteric vasculature bed injected with tumor necrosis factor  $\alpha$  (TNF- $\alpha$ ), a marked difference in binding to the endothelium was observed (Figures 6A–6C). Neutrophils devoid of polySia adhered to the vascular endothelium more tightly than WT neutrophils as evidenced by a greater number of stationary ST8SialIV<sup>-/-</sup> neutrophils present in venules of 20–50  $\mu$ m in diameter at all time periods examined (Figures 6A, 6C, and S5; Video S1). In addition, ST8SialIV<sup>-/-</sup> neutrophils were more likely than WT cells to roll along the endothelium (Figure 6B). Consistent with their tendency to adhere more tightly than WT cells to the endothelium, fewer ST8SialIV<sup>-/-</sup> neutrophils extravasated from the cremasteric vasculature in response to TNF- $\alpha$  (Figures 6D–6F), and they traveled a shorter distance than WT neutrophils (Figure 6E).

Thus, *in vivo* and *in vitro* data support a role of polySia in regulating chemokine-driven neutrophil migration as well as interaction with the vascular endothelium.

### PolySia expression on surface of myeloid cells is dynamically regulated during migration from bone marrow to lungs after infection with *Spn*

Having shown the effect of polysialylation on leukocyte migration and phagocytosis, we determined whether physiologic changes in cell-surface polySia on BM, PB, and BAL neutrophils and monocytes from WT mice during *Spn* infection were compatible with optimal immune function. We had previously demonstrated that cell-surface polySia was significantly lost from the surface of most murine neutrophils but from only a small subset of monocytes during migration from BM to PB under homeostatic conditions, and that most lung alveolar myeloid cells (Ly6 G/C<sup>+</sup>) were devoid of cell-surface polySia 24 h after lung instillation with LPS.<sup>16</sup> As seen in uninfected mice, most BM neutrophils and monocytes harvested 24 h and 48 h postinfection with *Spn* were polysialylated, and there was a significant decline in the

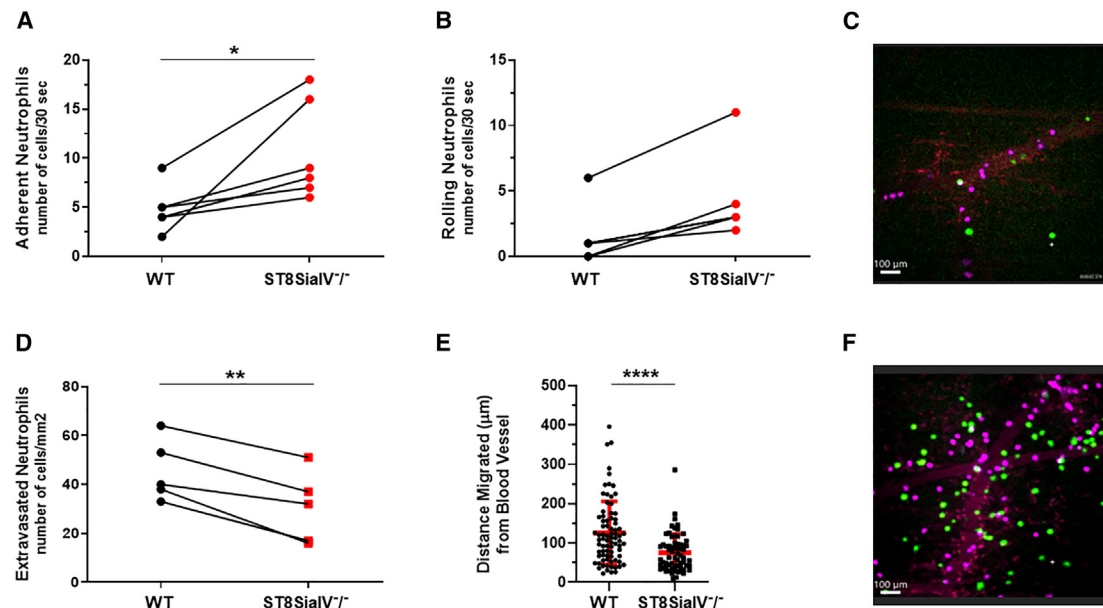


**Figure 6. ST8SialV<sup>-/-</sup> neutrophils are more adherent to and display reduced extravasation through the cremasteric microvasculature compared with WT cells**

ST8SialV<sup>-/-</sup> (magenta) and WT (green) BM neutrophils were prepared and injected into WT recipient mice.

(A–D) Adhesion to (A), rolling along (B), and extravasation through (C and D) the cremasteric vascular bed of labeled donor cells were observed by intravital microscopy as noted in STAR Methods. To induce recruitment of donor neutrophils in recipient WT mice, the cremasteric tissue was locally injected with TNF- $\alpha$  prior to cell transfusion. The number of adherent neutrophils (A) was determined by counting the stationary cells in a single 20- to 50- $\mu$ m diameter venule per microscopic field over 30-s frames. The number of rolling cells (B) comprised cells per main venule per microscopic field migrating up to 100  $\mu$ m per 30-s frame. A representative intravital microscopic image is shown in (C).

(D–F) The number of emigrated extravascular donor WT and ST8SialV<sup>-/-</sup> mouse neutrophils was measured per microscopic field from 0.5 to 2 h post cell transfusion (D). The distance traveled from the nearest blood vessel by these cells was measured using Imaris software (E). A representative intravital microscopic image of extravasated neutrophils is shown in (F).

Data acquired from 4–6 vascular beds from three different recipient WT mice are expressed as mean  $\pm$  SEM. \* $p \leq 0.05$ ; \*\* $p \leq 0.01$ ; \*\*\*\* $p \leq 0.0001$  (two-tailed t test). Scale bars, 100  $\mu$ m.

percentage of neutrophils expressing polySia from PB of all mice, as well as in the mean fluorescence intensity (MFI) of staining, at both time points (Figure 7A). In contrast to results from uninfected mice, however, there was a significant decline in both number and MFI of staining of polysialylated PB monocytes 24 h and 48 h postinfection (Figure 7B). Continued migration of neutrophils and monocytes into the alveolar spaces was associated with a further loss of cell-surface polySia (Figures 7A and 7B). Thus the downregulation, but not complete loss, of polySia expression on myeloid cells during migration from BM to lungs after pulmonary infection with *Spn* is consistent with maximizing migratory and phagocytic function of these cells during early infection.

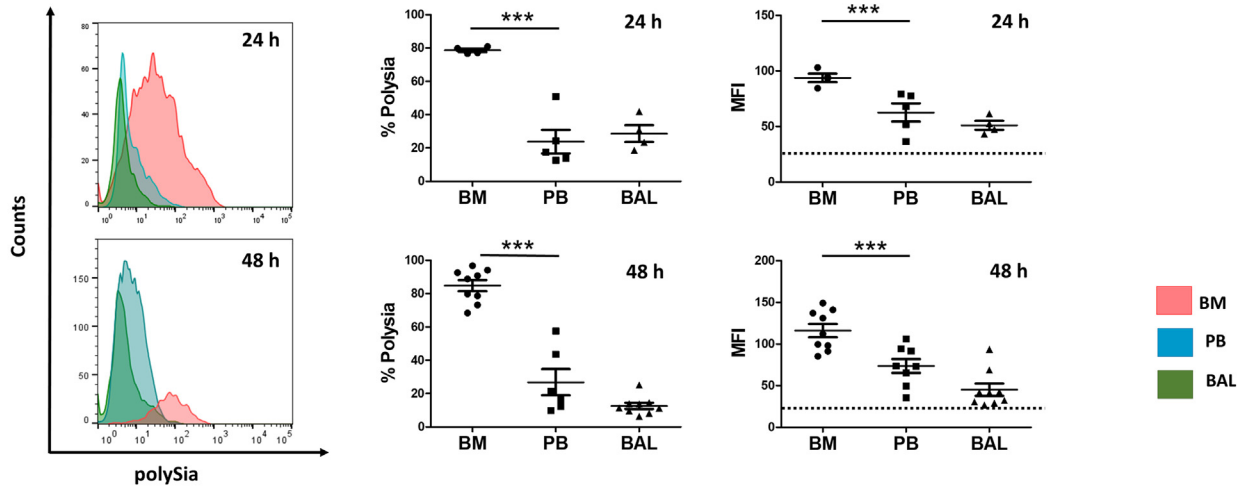
## DISCUSSION

It is well established that the dynamic regulation of polySia expression in neurons and glial cells guides the programmed development of the central nervous system.<sup>12,29</sup> In this report, we provide evidence that regulated expression of polySia on cells of the murine immune system similarly helps orchestrate an effective immune response to bacterial pulmonary infection. We demonstrate that the changing amount of polySia on the sur-

face of neutrophils and monocytes helps control chemokine-driven migration to a pulmonary focus of *Spn* infection as well as leukocyte adhesion to and extravasation through vascular endothelium. We also demonstrate that the absence of polySia on alveolar leukocytes promotes phagocytosis of *Spn* and prolongs cell longevity. These findings help explain the greater clearance of *Spn* from the lungs of infected ST8SialV<sup>-/-</sup> mice with less inflammatory damage to host tissue. The differences in leukocyte activity that we observed between WT and polySia-deficient cells may be related to an altered capacity to respond to extracellular signals, as we showed with ERK1/2 phosphorylation in response to fMLP. Given the greater survival of ST8SialV<sup>-/-</sup> mice compared with WT mice following *Spn* infection, it appears that enhanced phagocytosis by polySia-deficient leukocytes is at least one event that helps compensate for reduced cell recruitment. Our findings suggest that polySia may have multiple roles that are cell specific and protein specific, and change depending on the evolving requirements of the immune response.

As shown with other glycans,<sup>30</sup> polySia plays a role in migration of a wide range of cells including neurons, malignant cells, and leukocytes.<sup>7,12,18,19,31</sup> The mechanisms by which it promotes migration are still being determined and are likely related

## A Neutrophils



## B Monocytes

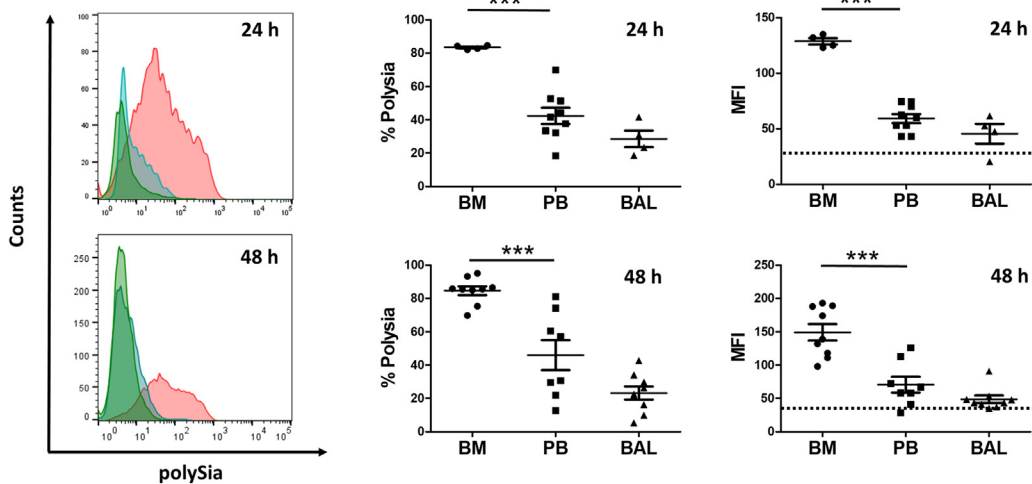


**Figure 7. PolySia is progressively lost from the surface of myeloid cells as they migrate from bone marrow to alveoli**

Neutrophils and monocytes were isolated from BM, PB, and alveolar spaces of *Spn*-infected WT and ST8SialV<sup>-/-</sup> mice 24 h and 48 h postinfection, stained with antibodies against CD45, CD11b, Ly6G, Ly6C, and polySia, and analyzed by flow cytometry. Histograms from individual mice (left panels) showing absolute cell counts as well as composite data from multiple mice showing percentage of cells polysialylated (middle panels) and MFI of staining (right panels) are presented for CD45-gated neutrophils (Ly6G/CD11b) (A) and monocytes (Ly6C/CD11b) (B) harvested at 24 h and 48 h postinfection (middle and right columns). Data represent mean  $\pm$  SEM (n = 4–9 mice) from four independent experiments. \*\*\*p  $\leq$  0.001 (two-tailed t test).

to its terminal location on glycans and its hydrophilic and electro-negative properties. These features help prevent inappropriate cell-cell interactions, provide recognition sites for ligand and receptor binding, and/or promote signaling through intracellular pathways.<sup>13</sup> Polysialylated DCs were previously shown to migrate more efficiently in response to LPS compared with polySia-deficient cells in *in vivo* and *in vitro* mouse migration studies.<sup>7,18,19</sup> A proposed mechanism was an induced conformational change in CCL21 after interacting with the polySia chain on CCR7 receptor that activated the autoinhibited chemokine.<sup>7</sup> It is noteworthy that CCL19, another CCR7 chemokine, did not demonstrate this effect, and that the amount of CCL21

bound to WT and ST8SialV<sup>-/-</sup> cells was not compared. We show in this study that polySia promotes migration of neutrophils toward structurally different chemoattractants, *f*MPL and CXCL1, which utilize distinct receptors.<sup>32,33</sup> The small molecular weight of *f*MPL makes a significant polySia-induced conformational change unlikely. In the case of CXCL1, enhanced migration of WT neutrophils was not a result of more chemokine bound to the cell surface, as neutrophils from ST8SialV<sup>-/-</sup> mice bound significantly more CXCL1 than did WT cells. Consistent with this finding, phosphorylation of ERK1/2 in ST8SialV<sup>-/-</sup> neutrophils was more robust than in WT cells after exposure to *f*MPL. Although *f*MPL-induced ERK1/2 signaling has been shown to

affect neutrophil migration in various ways,<sup>34,35</sup> our findings are consistent with the negative impact of excess chemoattractant binding on cell migration.<sup>34</sup> The greater amount of CXCL1 bound to polySia-deficient cells likely also dysregulated intracellular signaling pathways related to cell migration<sup>36,37</sup> and/or adversely affected cell velocity and persistence, as observed in the microfluidic chamber assays.

To establish that polySia specific to myeloid cells drives their migration during pulmonary infection, we adoptively transferred monocytes and neutrophils from ST8SialV<sup>-/-</sup> and WT mice into recipient WT mice. This eliminated the possible confounding influence on myeloid cell migration of polySia expressed by other cells, such as endothelial and lung epithelial cells<sup>38-40</sup> and of soluble polySia in serum.<sup>41</sup> As polySia was absent in these compartments in a previous study of DC trafficking in ST8SialV<sup>-/-</sup> mice,<sup>7</sup> it was not clear that the impairment in DC migration reported there was a result solely of the absence of polySia on DCs. The difference in migration of WT and polySia-deficient monocytes and neutrophils to the lungs of infected recipient WT mice that we observed was strictly the result of the polySia status of these cells.

Our comparative studies in ST8SialV<sup>-/-</sup> and WT mice provide insight into how the regulated expression of polySia during the activation, differentiation, and mobilization of murine BM neutrophils and monocytes contributes to the overall immune response against a pulmonary pathogen. Similar to what we showed previously using a peritoneal model of mouse inflammation,<sup>16</sup> in this report we demonstrate the progressive loss of polySia from BM leukocytes as they migrate to the lungs after infection with *Spn*. What might be the role of leukocytes losing polySia during the early immune response when our data show that cells from WT mice migrate more efficiently to infected lungs than do cells from ST8SialV<sup>-/-</sup> mice and have increased velocity and persistence *in vitro* compared with polySia-deficient cells? Progressive loss of polySia may help modulate chemokine binding. As we have shown that increased amounts of chemokine CXCL1 bind to BM neutrophils without cell-surface polySia (Figure 5), the loss of polySia may help increase binding of, and thus the response to, chemokines such as CXCL1. At the same time, there might still be enough of this bulky, electronegative glycan on the cell surface to prevent stalling of cells by inappropriate cell-cell contacts (Figure S5). Cellular responses to chemoattractants follow a bell-shaped concentration curve,<sup>36,37</sup> and retention of some polySia may prevent excessive chemokine binding that was seen with ST8SialV<sup>-/-</sup> neutrophils, with consequent loss of persistence and decreased velocity. Further removal of polySia as cells approach the site of infection, and further chemokine binding, might slow cell migration by altering intracellular signaling.<sup>34</sup> It might also diminish steric hindrance to a number of critical cell interactions that are needed for transendothelial migration as well as promote contact or recognition of microbes, such as *Spn*. These cell interactions would likely involve receptors other than well-recognized cell-adhesion selectin and integrin receptors that are dispensable for neutrophil recruitment during *Spn* infection.<sup>42</sup> Adverse consequences of complete loss of polySia include excessive adhesion of transfused ST8SialV<sup>-/-</sup> neutrophils to endothelium and impaired extravasation seen in our intravital microscopy studies. After

recruitment to the inflammatory site, leukocytes begin to regain polySia on different proteins, such as neuropilin-2.<sup>4,16,43</sup> This may be part of a mechanism to mute phagocytosis and switch to antigen presentation mode. Polysialylation of NRP-2 on mature DCs would then promote migration via other chemokines such as CCL21.<sup>7,18,19</sup>

Although WT leukocytes that have homed to the lungs have lost much of their cell-surface polySia and in that regard are similar to ST8SialV<sup>-/-</sup> leukocytes, these two sets of cells may differ in other ways. Intracellular polysialylated proteins have been described,<sup>9</sup> and these proteins may regulate intracellular processes and signaling pathways in WT leukocytes differently from ST8SialV<sup>-/-</sup> leukocytes that are devoid of these proteins. Secretion of polySia from these cells may also have a role in cell function by impacting interactions on the cell surface.<sup>9,40</sup> Lastly, these cells that appear to have similar cell-surface polySia content at the time of tissue homing may have been “programmed” differently because of differences in polysialylation at earlier stages of the immune response.

Control of polySia expression in cells of the immune system depends on the activity of polysialyltransferase ST8SialV<sup>4,17,18,43</sup> and/or the level of expression of carrier proteins. The display of cell-surface polySia may be regulated additionally by sialidases Neu1 and Neu4 that have been shown to degrade this sugar<sup>44-46</sup> and/or by proteolysis of a carrier protein that we showed reduced polySia expression on murine monocytes.<sup>16</sup> CD56/NCAM, CCR7 receptor, ESL-1, and NRP-2 are the proteins in the immune system currently known to express polySia.<sup>4,7,9,16,17</sup> Given that these proteins are commonly known to be involved in cell-cell interactions, it is possible that polySia modification regulates the function of these particular proteins, rather than these proteins being selected by the cell as carriers for polySia to achieve a more general cellular function. CD56/NCAM is the predominant polysialylated protein in murine BM monocytes and neutrophils, although monocytes express an additional polysialylated protein that remains to be identified.<sup>4</sup> Preliminary data from our laboratory using NCAM<sup>-/-</sup> mice show no difference in survival compared with WT mice after pulmonary infection with *Spn*, suggesting that the survival advantage of ST8SialV<sup>-/-</sup> mice is not related to the absence of polySia on NCAM but rather to this additional protein.

In contrast to the central nervous system of mice, where a large portion of NCAM is polysialylated early during development, only a small percentage of NCAM in BM leukocytes carries polySia, and that NCAM is cleaved as cells migrate into the PB. It remains to be determined whether and how this minor population of polysialylated NCAM functions differently from NCAM on neutrophils and monocytes that is not decorated by polySia. Although we speculate in this article that polySia in these cells may help control the binding of chemoattractants, we and others have not shown a difference in numbers of neutrophils and monocytes in the PB of WT and ST8SialV<sup>-/-</sup> mice.<sup>24</sup> As monocytes differentiate into macrophages and DCs, NCAM no longer carries polySia, and these cells regain polySia on NRP2, CCR7, ESL-1, and other proteins to be identified. The relative importance of polysialylated NCAM in BM leukocytes and of polySia on these other proteins during later stages of the immune response remains to be determined.

ST8SialV<sup>-/-</sup> mice more efficiently cleared encapsulated, type 3 *Pneumococcus* from the lungs than did infected WT mice. Although there are several potential explanations for this, such as altered adhesion to lung epithelial cells, more efficient phagocytosis by ST8SialV<sup>-/-</sup> alveolar leukocytes likely played a key role. This is consistent with our previous finding that removal of polySia from the surface of activated peritoneal macrophages enhanced phagocytosis of *K. pneumoniae*.<sup>16</sup> AMs comprise the predominant immune cell that encounters pulmonary microbial pathogens. Whether resident cells or derived from BM, AMs do not express cell-surface polySia in their resting steady state. However, polySia expression is upregulated in AMs in WT mice after exposure to *Spn*, possibly as a way to transition from a phagocytic to an antigen-presenting cell. Although macrophage phagocytosis is important at sites of infection, macrophages must also have the capacity to downregulate phagocytosis to proceed through the next stages of an inflammatory response, and addition of polySia may be one such mechanism. To obtain enough AMs to conduct *in vitro* phagocytosis assays, we activated AMs *in vivo* with LPS for 24 h, sufficient time to detect cell-surface polySia. Thus, the cells from WT and ST8SialV<sup>-/-</sup> mice in our assays differed in polySia content, whereas under physiological conditions *in vivo* there was no apparent difference between strains in amount of cell-surface polySia. On the other hand, intracellular polySia, which has been reported in THP-1 macrophages,<sup>9</sup> may influence the phagocytic activity of these cells, providing a more subtle difference between WT and ST8SialV<sup>-/-</sup> AMs. Possible mechanism(s) for enhanced phagocytosis of *Spn* by cells lacking cell-surface polySia include unmasking of specific cell-surface pathogen receptors, non-specific removal of repulsive negative charge on the cell surface that promotes microbe-cell interactions, and/or activation of intracellular signaling pathways.

Our work demonstrates that the programmed expression of the unique glycan polySia on neutrophils and monocytes plays a significant role in controlling the immune response during pneumococcal pneumonia. Although NCAM/CD56 is the predominant carrier of polySia in murine BM myeloid cells, it remains to be determined whether this or another polysialylated protein yet to be identified, or simply the polySia moiety itself, is responsible for the effects shown. We have focused our studies here on myeloid cells that play a prominent role in the early innate response to bacterial infection, yet lymphocytes also express polySia,<sup>23</sup> and their polysialylation status also likely impacts viral infections and other inflammatory states. The murine model of pneumonia is an excellent system in which to study the changing expression of polySia on immune cells during an evolving immune response, as there are many similarities in expression of polySia on human and murine leukocytes. The results from our studies will provide a blueprint to engineer levels of expression of polySia on subsets of leukocytes to optimize migration to and from sites of infection/inflammation and to improve the overall immune response. Our findings highlighting the role of a specific glycan extend to infection of extrapulmonary sites and to other disciplines in which clinical outcome is influenced by modulating the migration and cell-cell and cell-ligand interactions of cells of the immune system.

### Limitations of the study

Leukocyte migration to the site of inflammation is a complex process that involves multiple interactions with endothelial cells in various vascular beds. These cell interactions in the lung involve receptors other than well-recognized cell adhesion selectin and integrin receptors that appear to be dispensable for neutrophil recruitment during *Spn* infection.<sup>42</sup> The specific endothelial cell proteins with which polysialylated proteins interact remain to be determined, leaving a gap in our understanding of mechanisms controlling the impact of polySia on leukocyte-endothelial interactions.

NCAM is the predominant polysialylated protein on neutrophils, and polySia, with or without NCAM on these cells, is likely responsible for the effects that we report. Monocytes, however, express polysialylated NCAM, which is partly removed from cells as they migrate from BM to PB, and an additional polysialylated protein(s) that appears to remain stable during cell migration. Identifying this protein will help us understand the mechanistic role of polySia in monocyte function.

Our study focuses on the early innate immune response to lung infection with a lethal dose of *Spn*. In light of the survival data with WT mice shown in Figure 1, we determined the residual bacterial burden in the lungs of WT and ST8SialV<sup>-/-</sup> mice 24 h postinfection and the level of cytokines and infiltrating leukocytes up to 48 h following infection. We did not analyze later times postinfection but assumed that the trends that we found would continue. As it is well recognized that activated macrophages and DCs, as well as lymphocytes, are polysialylated, the adaptive immune response in ST8SialV<sup>-/-</sup> mice to a sublethal dose of *Spn* remains to be determined.

Our methods for obtaining sufficient numbers of alveolar and peritoneal macrophages (LPS versus thioglycolate stimulation) as well as their inherent differences and the differences in phagocytosis assays (adherent peritoneal macrophages versus AMs in solution; different multiplicities of infection with *Spn* with each population of cells) make direct quantitative comparisons of function between these two types of morphologically and functionally distinct subsets of macrophages difficult.

Although endoN glycosidase treatment effectively removes polySia from the cell surface, the activity of these treated cells may still be influenced by intracellular polySia<sup>9</sup> and/or by trace amounts of polySia that are below the level of detection by flow cytometry. Thus, endoN-treated WT macrophages may not be expected to act identically to ST8SialV<sup>-/-</sup> macrophages.

### STAR★METHODS

Detailed methods are provided in the online version of this paper and include the following:

- KEY RESOURCES TABLE
- RESOURCE AVAILABILITY
  - Lead contact
  - Materials availability
  - Data and code availability
- EXPERIMENTAL MODEL AND STUDY PARTICIPANT DETAILS

- Mice
- Bacterial strain
- **METHOD DETAILS**
  - Infection
  - Isolation of bone marrow and peripheral blood leukocytes
  - Bronchoalveolar lavage and lung homogenization
  - Analysis of lung tissue
  - Flow cytometry
  - Adoptive transfer of WT and ST8SialV<sup>-/-</sup> leukocytes
  - Cytokine measurement in lung homogenates
  - Measurement of cell-bound cytokine and amount of total and phosphorylated ERK1/2
  - Immunoblot analysis of cellular proteins
  - Phagocytosis assay of peritoneal and alveolar cells
  - Transwell cell migration assay
  - Intravital microscopy of cremasteric microcirculation
  - Apoptosis assay
- **QUANTIFICATION AND STATISTICAL ANALYSIS**

#### SUPPLEMENTAL INFORMATION

Supplemental information can be found online at <https://doi.org/10.1016/j.celrep.2023.112648>.

#### ACKNOWLEDGMENTS

This work was supported by National Institutes of Health grants 5R01AI132733 (N.M.S.), R01 CA254193 (K.K.), and R01 GM134542 (K.K.), and postdoctoral fellowships from the Fonds de recherche du Québec – Nature et technologies and the Natural Sciences and Engineering Research Council of Canada (A.K.). We are grateful to Minoru Fukuda (The Burnham Institute, La Jolla, CA) for generously providing breeding pairs of ST8SialV<sup>-/+</sup> mice and to Joseph Mauban (Center for Innovative Biomedical Resources, University of Maryland School of Medicine; NIH-ORIP: S10 RR032977) for assistance with intravital microscopy.

#### AUTHOR CONTRIBUTIONS

N.M.S. conceptualized and supervised the study and acquired financial support. P.S., A.K., L.Z., S.S., and N.M.S. planned and performed experiments and analyzed data. A.K. conducted microfluidic migration assays and analyzed results. K.K. supervised and financially supported microfluidic migration assays. L.Z. managed mouse breeding and provided mice for experiments. P.S. and N.M.S. wrote the manuscript.

#### DECLARATION OF INTERESTS

The authors declare no competing interests.

Received: November 1, 2022

Revised: April 13, 2023

Accepted: May 31, 2023

#### REFERENCES

1. Mandell, L.A., Wunderink, R.G., Anzueto, A., Bartlett, J.G., Campbell, G.D., Dean, N.C., Dowell, S.F., File, T.M., Jr., Musher, D.M., Niederman, M.S., et al. (2007). Infectious Diseases Society of America/American Thoracic Society consensus guidelines on the management of community-acquired pneumonia in adults. *Clin. Infect. Dis.* *44*, S27–S72. <https://doi.org/10.1086/511159>.
2. Chang, Y.C., and Nizet, V. (2014). The interplay between Siglecs and sialylated pathogens. *Glycobiology* *24*, 818–825. <https://doi.org/10.1093/glycob/cwu067>.
3. Close, B.E., and Colley, K.J. (1998). In vivo autopolysialylation and localization of the polysialyltransferases PST and STX. *J. Biol. Chem.* *273*, 34586–34593. <https://doi.org/10.1074/jbc.273.51.34586>.
4. Curreli, S., Arany, Z., Gerardy-Schahn, R., Mann, D., and Stamos, N.M. (2007). Polysialylated neuropilin-2 is expressed on the surface of human dendritic cells and modulates dendritic cell-T lymphocyte interactions. *J. Biol. Chem.* *282*, 30346–30356. <https://doi.org/10.1074/jbc.M702965200>.
5. Finne, J. (1982). Occurrence of unique polysialosyl carbohydrate units in glycoproteins of developing brain. *J. Biol. Chem.* *257*, 11966–11970.
6. Galuska, S.P., Rollenhagen, M., Kaup, M., Eggers, K., Oltmann-Norden, I., Schiff, M., Hartmann, M., Weinhold, B., Hildebrandt, H., Geyer, R., et al. (2010). Synaptic cell adhesion molecule SynCAM 1 is a target for polysialylation in postnatal mouse brain. *Proc. Natl. Acad. Sci. USA* *107*, 10250–10255. <https://doi.org/10.1073/pnas.0912103107>.
7. Kiermaier, E., Moussion, C., Veldkamp, C.T., Gerardy-Schahn, R., de Vries, I., Williams, L.G., Chaffee, G.R., Phillips, A.J., Freiberger, F., Imre, R., et al. (2016). Polysialylation controls dendritic cell trafficking by regulating chemokine recognition. *Science* *351*, 186–190. <https://doi.org/10.1126/science.aad0512>.
8. Mühlhoff, M., Eckhardt, M., Bethe, A., Frosch, M., and Gerardy-Schahn, R. (1996). Autocatalytic polysialylation of polysialyltransferase-1. *EMBO J.* *15*, 6943–6950.
9. Werneburg, S., Buettner, F.F.R., Erben, L., Mathews, M., Neumann, H., Mühlhoff, M., and Hildebrandt, H. (2016). Polysialylation and lipopolysaccharide-induced shedding of E-selectin ligand-1 and neuropilin-2 by microglia and THP-1 macrophages. *Glia* *64*, 1314–1330. <https://doi.org/10.1002/glia.23004>.
10. Yabe, U., Sato, C., Matsuda, T., and Kitajima, K. (2003). Polysialic acid in human milk. CD36 is a new member of mammalian polysialic acid-containing glycoprotein. *J. Biol. Chem.* *278*, 13875–13880. <https://doi.org/10.1074/jbc.M300458200>.
11. Zuber, C., Lackie, P.M., Catterall, W.A., and Roth, J. (1992). Polysialic acid is associated with sodium channels and the neural cell adhesion molecule N-CAM in adult rat brain. *J. Biol. Chem.* *267*, 9965–9971.
12. Rutishauser, U. (2008). Polysialic acid in the plasticity of the developing and adult vertebrate nervous system. *Nat. Rev. Neurosci.* *9*, 26–35. <https://doi.org/10.1038/nrn2285>.
13. Thiesler, H., Küçükerden, M., Gretenkort, L., Röckle, I., and Hildebrandt, H. (2022). News and views on polysialic acid: from tumor progression and brain development to psychiatric disorders, neurodegeneration, myelin repair and immunomodulation. *Front. Cell Dev. Biol.* *10*, 871757. <https://doi.org/10.3389/fcell.2022.871757>.
14. Villanueva-Cabello, T.M., Gutiérrez-Valenzuela, L.D., Salinas-Marín, R., López-Guerrero, D.V., and Martínez-Duncker, I. (2021). Polysialic acid in the immune system. *Front. Immunol.* *12*, 823637. <https://doi.org/10.3389/fimmu.2021.823637>.
15. Rollenhagen, M., Buettner, F.F.R., Reismann, M., Jirmo, A.C., Grove, M., Behrens, G.M.N., Gerardy-Schahn, R., Hanisch, F.G., and Mühlhoff, M. (2013). Polysialic acid on neuropilin-2 is exclusively synthesized by the polysialyltransferase ST8SialV and attached to mucin-type o-glycans located between the b2 and c domain. *J. Biol. Chem.* *288*, 22880–22892. <https://doi.org/10.1074/jbc.M113.463927>.
16. Stamos, N.M., Zhang, L., Jokilampi, A., Finne, J., Chen, W.H., El-Maarouf, A., Cross, A.S., and Hankey, K.G. (2014). Changes in polysialic acid expression on myeloid cells during differentiation and recruitment to sites of inflammation: role in phagocytosis. *Glycobiology* *24*, 864–879. <https://doi.org/10.1093/glycob/cwu050>.
17. Drake, P.M., Nathan, J.K., Stock, C.M., Chang, P.V., Muench, M.O., Nakata, D., Reader, J.R., Gip, P., Golden, K.P.K., Weinhold, B., et al.

- (2008). Polysialic acid, a glycan with highly restricted expression, is found on human and murine leukocytes and modulates immune responses. *J. Immunol.* *181*, 6850–6858. <https://doi.org/10.4049/jimmunol.181.10.6850>.
18. Bax, M., van Vliet, S.J., Litjens, M., García-Vallejo, J.J., and van Kooyk, Y. (2009). Interaction of polysialic acid with CCL21 regulates the migratory capacity of human dendritic cells. *PLoS One* *4*, e6987. <https://doi.org/10.1371/journal.pone.0006987>.
  19. Rey-Gallardo, A., Delgado-Martín, C., Gerardy-Schahn, R., Rodríguez-Fernández, J.L., and Vega, M.A. (2011). Polysialic acid is required for neuropilin-2a/b-mediated control of CCL21-driven chemotaxis of mature dendritic cells and for their migration in vivo. *Glycobiology* *21*, 655–662. <https://doi.org/10.1093/glycob/cwq216>.
  20. Rey-Gallardo, A., Escribano, C., Delgado-Martín, C., Rodríguez-Fernández, J.L., Gerardy-Schahn, R., Rutishauser, U., Corbi, A.L., and Vega, M.A. (2010). Polysialylated neuropilin-2 enhances human dendritic cell migration through the basic C-terminal region of CCL21. *Glycobiology* *20*, 1139–1146. <https://doi.org/10.1093/glycob/cwq078>.
  21. Thiesler, H., Beimdiek, J., and Hildebrandt, H. (2021). Polysialic acid and Siglec-E orchestrate negative feedback regulation of microglia activation. *Cell. Mol. Life Sci.* *78*, 1637–1653. <https://doi.org/10.1007/s00018-020-03601-z>.
  22. Wang, Y., and Neumann, H. (2010). Alleviation of neurotoxicity by microglial human Siglec-11. *J. Neurosci.* *30*, 3482–3488. <https://doi.org/10.1523/JNEUROSCI.3940-09.2010>.
  23. Villanueva-Cabello, T.M., Gutiérrez-Valenzuela, L.D., López-Guerrero, D.V., Cruz-Muñoz, M.E., Mora-Montes, H.M., and Martínez-Duncker, I. (2019). Polysialic acid is expressed in human naive CD4+ T cells and is involved in modulating activation. *Glycobiology* *29*, 557–564. <https://doi.org/10.1093/glycob/cwz032>.
  24. Drake, P.M., Stock, C.M., Nathan, J.K., Gip, P., Golden, K.P.K., Weinhold, B., Gerardy-Schahn, R., and Bertozzi, C.R. (2009). Polysialic acid governs T-cell development by regulating progenitor access to the thymus. *Proc. Natl. Acad. Sci. USA* *106*, 11995–12000. <https://doi.org/10.1073/pnas.0905188106>.
  25. Angata, K., Huckaby, V., Ranscht, B., Terskikh, A., Marth, J.D., and Fukuda, M. (2007). Polysialic acid-directed migration and differentiation of neural precursors are essential for mouse brain development. *Mol. Cell Biol.* *27*, 6659–6668. <https://doi.org/10.1128/MCB.00205-07>.
  26. Ulm, C., Saffarzadeh, M., Mahavadi, P., Müller, S., Prem, G., Saboor, F., Simon, P., Middendorff, R., Geyer, H., Henneke, I., et al. (2013). Soluble polysialylated NCAM: a novel player of the innate immune system in the lung. *Cell. Mol. Life Sci.* *70*, 3695–3708. <https://doi.org/10.1007/s00018-013-1342-0>.
  27. Finne, J., and Mäkelä, P.H. (1985). Cleavage of the polysialosyl units of brain glycoproteins by a bacteriophage endosialidase. Involvement of a long oligosaccharide segment in molecular interactions of polysialic acid. *J. Biol. Chem.* *260*, 1265–1270.
  28. Rutishauser, U., Watanabe, M., Silver, J., Troy, F.A., and Vimr, E.R. (1985). Specific alteration of NCAM-mediated cell adhesion by an endoneuraminidase. *J. Cell Biol.* *101*, 1842–1849. <https://doi.org/10.1083/jcb.101.5.1842>.
  29. Schnaar, R.L., Gerardy-Schahn, R., and Hildebrandt, H. (2014). Sialic acids in the brain: gangliosides and polysialic acid in nervous system development, stability, disease, and regeneration. *Physiol. Rev.* *94*, 461–518. <https://doi.org/10.1152/physrev.00033.2013>.
  30. Wright, R.D., and Cooper, D. (2014). Glycobiology of leukocyte trafficking in inflammation. *Glycobiology* *24*, 1242–1251. <https://doi.org/10.1093/glycob/cwu101>.
  31. Seifert, A., Glanz, D., Glaubitz, N., Horstkorte, R., and Bork, K. (2012). Polysialylation of the neural cell adhesion molecule: interfering with polysialylation and migration in neuroblastoma cells. *Arch. Biochem. Biophys.* *524*, 56–63. <https://doi.org/10.1016/j.abb.2012.04.011>.
  32. Haribabu, B., Richardson, R.M., Verghese, M.W., Barr, A.J., Zhelev, D.V., and Snyderman, R. (2000). Function and regulation of chemoattractant receptors. *Immunol. Res.* *22*, 271–279. <https://doi.org/10.1385/IR:22:2-3>.
  33. Metzemaekers, M., Gouwy, M., and Proost, P. (2020). Neutrophil chemoattractant receptors in health and disease: double-edged swords. *Cell. Mol. Immunol.* *17*, 433–450. <https://doi.org/10.1038/s41423-020-0412-0>.
  34. Liu, X., Ma, B., Malik, A.B., Tang, H., Yang, T., Sun, B., Wang, G., Minshall, R.D., Li, Y., Zhao, Y., et al. (2012). Bidirectional regulation of neutrophil migration by mitogen-activated protein kinases. *Nat. Immunol.* *13*, 457–464. <https://doi.org/10.1038/ni.2258>.
  35. Zhang, E.R., Liu, S., Wu, L.F., Altschuler, S.J., and Cobb, M.H. (2016). Chemoattractant concentration-dependent tuning of ERK signaling dynamics in migrating neutrophils. *Sci. Signal.* *9*, ra122. <https://doi.org/10.1126/scisignal.aag0486>.
  36. Bonecchi, R., Polentarutti, N., Luini, W., Borsatti, A., Bernasconi, S., Locati, M., Power, C., Proudfoot, A., Wells, T.N., Mackay, C., et al. (1999). Up-regulation of CCR1 and CCR3 and induction of chemotaxis to CC chemokines by IFN- $\gamma$  in human neutrophils. *J. Immunol.* *162*, 474–479.
  37. Khajah, M., Millen, B., Cara, D.C., Waterhouse, C., and McCafferty, D.M. (2011). Granulocyte-macrophage colony-stimulating factor (GM-CSF): a chemoattractive agent for murine leukocytes in vivo. *J. Leukoc. Biol.* *89*, 945–953. <https://doi.org/10.1189/jlb.0809546>.
  38. Park, H., Pagan, L., Tan, O., Fadiel, A., Demir, N., Huang, K., Mittal, K., and Naftolin, F. (2010). Estradiol regulates expression of polysialated neural cell adhesion molecule by human vascular endothelial cells. *Reprod. Sci.* *17*, 1090–1098. <https://doi.org/10.1177/1933719110379649>.
  39. Strubl, S., Schubert, U., Kühnle, A., Rebl, A., Ahmadvand, N., Fischer, S., Preissner, K.T., and Galuska, S.P. (2018). Polysialic acid is released by human umbilical vein endothelial cells (HUVEC) in vitro. *Cell Biosci.* *8*, 64. <https://doi.org/10.1186/s13578-018-0262-y>.
  40. Das, S., MacDonald, K., Chang, H.Y.S., and Mitzner, W. (2013). A simple method of mouse lung intubation. *J. Vis. Exp.*, e50318. <https://doi.org/10.3791/50318>.
  41. Tajik, A., Phillips, K.L., Nitz, M., and Willis, L.M. (2020). A new ELISA assay demonstrates sex differences in the concentration of serum polysialic acid. *Anal. Biochem.* *600*, 113743. <https://doi.org/10.1016/j.ab.2020.113743>.
  42. Palmer, C.S., and Kimmey, J.M. (2022). Neutrophil recruitment in pneumococcal pneumonia. *Front. Cell. Infect. Microbiol.* *12*, 894644. <https://doi.org/10.3389/fcimb.2022.894644>.
  43. Mühlenhoff, M., Rollenhagen, M., Werneburg, S., Gerardy-Schahn, R., and Hildebrandt, H. (2013). Polysialic acid: versatile modification of NCAM, SynCAM 1 and neuropilin-2. *Neurochem. Res.* *38*, 1134–1143. <https://doi.org/10.1007/s11064-013-0979-2>.
  44. Abe, C., Yi, Y., Hane, M., Kitajima, K., and Sato, C. (2019). Acute stress-induced change in polysialic acid levels mediated by sialidase in mouse brain. *Sci. Rep.* *9*, 9950. <https://doi.org/10.1038/s41598-019-46240-6>.
  45. Sumida, M., Hane, M., Yabe, U., Shimoda, Y., Pearce, O.M.T., Kiso, M., Miyagi, T., Sawada, M., Varki, A., Kitajima, K., and Sato, C. (2015). Rapid trimming of cell surface polysialic acid (PolySia) by exovesicular sialidase triggers release of preexisting surface neurotrophin. *J. Biol. Chem.* *290*, 13202–13214. <https://doi.org/10.1074/jbc.M115.638759>.
  46. Takahashi, K., Mitoma, J., Hosono, M., Shiozaki, K., Sato, C., Yamaguchi, K., Kitajima, K., Higashi, H., Nitta, K., Shima, H., and Miyagi, T. (2012). Sialidase NEU4 hydrolyzes polysialic acids of neural cell adhesion molecules and negatively regulates neurite formation by hippocampal neurons. *J. Biol. Chem.* *287*, 14816–14826. <https://doi.org/10.1074/jbc.M111.324186>.
  47. Angata, K., Long, J.M., Bukalo, O., Lee, W., Dityatev, A., Wynshaw-Boris, A., Schachner, M., Fukuda, M., and Marth, J.D. (2004). Sialyltransferase ST8Sia-II assembles a subset of polysialic acid that directs hippocampal

- axonal targeting and promotes fear behavior. *J. Biol. Chem.* 279, 32603–32613. <https://doi.org/10.1074/jbc.M403429200>.
48. Nelson, A.M., Nolan, K.E., and Davis, I.C. (2020). Repeated orotracheal intubation in mice. *J. Vis. Exp.* <https://doi.org/10.3791/60844>.
49. Swamydas, M., Luo, Y., Dorf, M.E., and Lionakis, M.S. (2015). Isolation of mouse neutrophils. *Curr. Protoc. Im.* 110, 3.20.15–23.20.15. <https://doi.org/10.1002/0471142735.im0320s110>.
50. Matute-Bello, G., Downey, G., Moore, B.B., Groshong, S.D., Matthay, M.A., Slutsky, A.S., and Kuebler, W.M.; Acute Lung Injury in Animals Study Group (2011). An official American Thoracic Society workshop report: features and measurements of experimental acute lung injury in animals. *Am. J. Respir. Cell Mol. Biol.* 44, 725–738. <https://doi.org/10.1165/rcmb.2009-0210ST>.
51. Hung, W.C., Chen, S.H., Paul, C.D., Stroka, K.M., Lo, Y.C., Yang, J.T., and Konstantopoulos, K. (2013). Distinct signaling mechanisms regulate migration in unconfined versus confined spaces. *J. Cell Biol.* 202, 807–824. <https://doi.org/10.1083/jcb.201302132>.
52. Tong, Z., Balzer, E.M., Dallas, M.R., Hung, W.C., Stebe, K.J., and Konstantopoulos, K. (2012). Chemotaxis of cell populations through confined spaces at single-cell resolution. *PLoS One* 7, e29211. <https://doi.org/10.1371/journal.pone.0029211>.
53. Wang, P., Chen, S.H., Hung, W.C., Paul, C., Zhu, F., Guan, P.P., Huso, D.L., Kontrogianni-Konstantopoulos, A., and Konstantopoulos, K. (2015). Fluid shear promotes chondrosarcoma cell invasion by activating matrix metalloproteinase 12 via IGF-2 and VEGF signaling pathways. *Oncogene* 34, 4558–4569. <https://doi.org/10.1038/ncr.2014.397>.

## STAR★METHODS

### KEY RESOURCES TABLE

REAGENT or RESOURCE	SOURCE	IDENTIFIER
<b>Antibodies</b>		
Anti-mouse Ly-6G antibody (clone 1A8)	Biolegend	Cat# 127614; RRID:AB_2227348
Anti-mouse Ly-6C antibody (clone AL-21)	BD Pharmingen	Cat# 560595; RRID:AB_1727554
Anti-mouse CD45 (clone 30-F11)	Biolegend	Cat# 103134; RRID:AB_2562559
Anti-mouse CD11b (clone M1/70)	Biolegend	Cat# 101208; RRID:AB_312791
Anti-mouse CD11c (clone)	BD Pharmingen	Cat# 550261; RRID:AB_398460
F(ab') <sub>2</sub> -goat Anti-rabbit IgG (h+) Cross-adsorbed Secondary Antibody, Alexa Fluor 488	Invitrogen	Cat# A11070; RRID:AB_2534114
anti-polySia mAb 735	Absolute Antibody	Cat# Ab00240-23.0; RRID:AB_2891042
anti-mouse F4/80 antibody (clone BM8)	Biolegend	Cat# 123128; RRID:AB_893484
anti-mouse CD170 (Siglec-F) antibody, (clone S17007L)	Biolegend	Cat# 155509; RRID:AB_2810421
anti-mouse CD182 (CXCR2) antibody (clone SA044G4)	Biolegend	Cat# 149310; RRID:AB_2566148
Rabbit anti Streptococcus pneumoniae	Biorad	Cat# 0300-0218; RRID:AB_620715
p44/42 MAPK (Erk1/2) Antibody	Cell Signaling Technology	Cat# 9102S; RRID:AB_330744
ERK 1/2 Antibody (MK1)	Santa Cruz Biotechnology	Cat# sc-135900; RRID:AB_2141283
Rabbit IgG Horseradish Peroxidase-conjugated Antibody	R&D systems	Cat# HAF008; RRID:AB_357235
Mouse-IgG Fc BP-HRP conjugated	Santa Cruz Biotechnology	Cat# sc525409
<b>Chemicals, peptides, and recombinant proteins</b>		
Todd Hewitt broth	sigma aldrich	Cat# T1438
Yeast Extract	sigma aldrich	Cat# Y1625
Isoflurane	VETone	Cat# 501017
Collagenase D, from Clostridium Histolyticum	sigma aldrich	Cat# 11088858001
DNase I from bovine pancreas	sigma aldrich	Cat# 11284932001
Formalin solution, neutral buffered, 10%	sigma aldrich	Cat# HT501128
Histopaque®-1077 Hybri-Max™	sigma aldrich	Cat# H8889
Histopaque®-1119	sigma aldrich	Cat# 11191
Recombinant Mouse CXCL1/KC Protein	R&D systems	Cat# 453-KC-010/CF
Mouse Monocyte Chemotactic Protein-1 (CCL2)	GeminiBio	Cat# 300-336P
Baby Rabbit Complement	Biorad	Cat# C12CA
N-Formyl-Met-Leu-Phe	sigma aldrich	Cat# F3506-5MG
CellTracker™ Deep Red Dye	Invitrogen	Cat# C34565
Vybrant™ CFDA SE Cell Tracer	Invitrogen	Cat# V12883
<b>Critical commercial assays</b>		
EasySep™ Mouse Monocyte Isolation Kit	stemcell technologies	Cat# 19861
Mouse CXCL1/KC Quantikine ELISA Kit	R&D systems	Cat# MKC00B
Mouse TGF-beta 1 DuoSet ELISA	R&D systems	Cat# DY1679-05
Mouse IL-1 beta/IL-1F2 DuoSet ELISA	R&D systems	Cat# DY401-05
Mouse CCL2/JE/MCP-1 Quantikine ELISA Kit	R&D systems	Cat# MJE00B
Mouse IL-10 Quantikine ELISA Kit	R&D systems	Cat# M1000B-1
QCM Chemotaxis Cell Migration Assay, 96-well (5 μm), fluorimetric	sigma aldrich	Cat# ECM512

(Continued on next page)

**Continued**

REAGENT or RESOURCE	SOURCE	IDENTIFIER
<b>Experimental models: Organisms/strains</b>		
Mouse, C57BL/6	The Jackson Laboratory	RRID:IMSR_JAX:000664
MouseST8 Sia II <sup>-/-</sup>	The Jackson Laboratory	RRID:IMSR_JAX:006902
Mouse, ST8Sia IV <sup>-/-</sup>	Gift from Minoru Fukuda (The Burnham Institute, La Jolla, CA) (Angata, Mol and Cell Biol, 2007)	NA
Serotype 3 <i>Streptococcus pneumoniae</i> ( <i>Spn</i> ) strain 6303	ATCC	Strain designation: [CIP 104225]
<b>Software and algorithms</b>		
FlowJo v10.2	Tree Star	<a href="https://www.flowjo.com/">https://www.flowjo.com/</a>
Prism v6.05	GraphPad	<a href="https://www.graphpad.com/scientificsoftware/prism/">https://www.graphpad.com/scientificsoftware/prism/</a>
<b>Other</b>		
blood agar plates	Hardy Diagnostics	Cat# A10
20 gauge catheter	Exel International	Cat# 14-841-17

**RESOURCE AVAILABILITY**

**Lead contact**

Further information and requests for resources and reagents should be directed to and will be fulfilled by lead contact Nicholas Stamatatos ([nstamatatos@ihv.umaryland.edu](mailto:nstamatatos@ihv.umaryland.edu)).

**Materials availability**

The ST8SiaIV<sup>-/-</sup> mice used in this study was a kind gift from Minoru Fukuda, and there are restrictions to the availability of this mouse based on an MTA with the Burnham Institute, La Jolla, CA. This study did not generate new reagents.

**Data and code availability**

- All data reported in this paper will be shared by the [lead contact](#) upon request.
- This paper does not report original code
- Any additional information required to reanalyze the data reported in this paper is available from the [lead contact](#) upon request.

**EXPERIMENTAL MODEL AND STUDY PARTICIPANT DETAILS**

**Mice**

C57BL/6 wild-type (WT; stock # 000664) and polysialyltransferase II-deficient (ST8Siall<sup>-/-</sup>; B6.129-St8sia2<sup>tm1Jxm</sup>/J; stock # 006902)<sup>47</sup> mice were purchased from the Jackson Laboratory (Bar Harbor, ME). ST8SiaIV<sup>-/-</sup> mice were a kind gift from Minoru Fukuda (The Burnham Institute, La Jolla, CA).<sup>25</sup> Eight to twelve week old, sex- and age-matched mice, bred on the C57BL/6 background, were maintained under pathogen-free conditions and strict 12 h light/dark cycling in the Animal Facility at the Institute of Human Virology and were used in all experiments. All animal care and experiments were conducted following procedures that were approved by the Institutional Animal Care and Use Committee of University of Maryland School of Medicine, Baltimore, MD.

**Bacterial strain**

Serotype 3 *Streptococcus pneumoniae* (*Spn*) strain 6303 (American Type Culture Collection, Manassas, VA) was used throughout this study. The bacteria was grown in Todd Hewitt broth containing 0.5% yeast extract (both from Sigma-Aldrich, St. Louis, MO) to mid-exponential phase in 5% CO<sub>2</sub> at 37 C, washed 2 times with PBS, and diluted in PBS to a concentration of 2 x 10<sup>5</sup> CFU/mL. The actual concentration of bacteria was confirmed in each experiment by plating 0.010 mL of serial dilutions of the inoculum on 5% blood agar plates (Hardy Diagnostics, Santa Maria, CA) and determining the number of single colonies after 16 h growth at 5% CO<sub>2</sub> and 37 C.

## METHOD DETAILS

### Infection

Intratracheal inoculation with *Spn* was performed combining select features of several recently described methods of mouse lung intubation.<sup>40,48</sup> Briefly, mice were anesthetized with 4% isoflurane (VETone, Boise, ID) and 2% O<sub>2</sub> delivered by a regulated isoflurane vaporizer (VETequip, Livermore, CA), fur was removed from the chest by depilatory cream and mice were suspended by the upper incisors facing up on an angled (60–80°) procedure board. A fiber optic cable was guided through a 20 gauge catheter (Exel International, QC, Canada), the tongue was retracted and the catheter was positioned in the trachea which was clearly visualized through the chest wall by transillumination. The fiber optic cable was removed and 50  $\mu$ l of bacterial inoculum ( $10^4$  CFU) was injected into the catheter and was fully aspirated on inhalation. Mice were held vertically for 30–40 s after the inoculation and observed until consciousness was regained. Mice were observed daily for clinical signs of moribundity as per IACUC guidelines.

### Isolation of bone marrow and peripheral blood leukocytes

Bone marrow cells were harvested from the femurs of 8–12 week-old mice and were used as source of monocytes and neutrophils in all experiments. Monocytes were purified from bone marrow cells by negative selection using an EasySep Mouse Monocyte Isolation Kit (Stem Cell Technologies, Vancouver, BC, Canada) as per the manufacturer's suggested protocol. Neutrophils were purified from bone marrow cells using Histopaque-based density gradient centrifugation.<sup>49</sup> Peripheral blood leukocytes were isolated from mice by collecting retro-orbital blood into a heparin-coated blood collection tube, diluting it 9-fold with ACK solution at 4°C, incubating for 3 min on ice, diluting 10-fold in PBS, and collecting the cells by centrifugation at 400 x g.

### Bronchoalveolar lavage and lung homogenization

Bronchoalveolar lavage (BAL) was performed at indicated times postinfection with *Spn* to analyze cellular composition and to measure residual *Spn* colony forming units (CFU). Mice were euthanized, the trachea was exposed and an incision was made through which a metal 18 gauge catheter was placed and tightly secured with suture. Lungs were then inflated with 1 mL of 4°C PBS which was aspirated and washed 2 additional times with 1 mL PBS. Cells were collected by centrifugation at 300 x g for 10 min, and the supernatant was removed for analysis of CFU. To prepare mouse lung homogenates, mice were euthanized and lungs were excised, digested in PBS containing 5% fetal calf serum (R&D Systems, Minneapolis, MN), 5,000 U/ml collagenase type D (Worthington Biochemicals, Lakewood, NJ) and 20 U/ml DNase (MilliporeSigma, Burlington, MA) at 37°C for 30 min to obtain a single cell suspension.

### Analysis of lung tissue

Immunohistochemistry was performed by perfusing harvested lungs with 10% buffered formalin (Sigma-Aldrich, Saint Louis, MO) for 1 h at room temperature. Fixed lungs were embedded in paraffin, cut into 10  $\mu$ m sections, mounted on glass slides, and stained with hematoxylin and eosin (H&E). The following parameters were assessed independently in each field by a pathologist who was blinded to sample identity: number of neutrophils in the alveolar (A) and interstitial (B) spaces; (C) number of hyaline membranes and (D) proteinaceous debris filling the airspaces and (E) areas of alveolar septal thickening. A final lung injury score was obtained using the following equation, as described elsewhere<sup>50</sup>:  $[(20 \times A) + (14 \times B) + (7 \times C) + (7 \times D) + (2 \times E)] / (\text{number of fields} \times 100)$ .

### Flow cytometry

Proteins and polySia on the surface of cells were detected by incubating cells at  $1 \times 10^6$  cells/ml in PBS containing 2% heat-inactivated human AB serum (R&D Systems, MN) at 4°C for 15 min to minimize nonspecific binding of reagents. Cells were stained with 10  $\mu$ g/ml rabbit anti-polySia mAb 735 (Absolute Antibody, Boston, MA) followed by FITC-conjugated F(ab')<sub>2</sub> anti-Rabbit IgG (Invitrogen, ThermoFisher Scientific, Carlsbad, CA). As control, cells were first treated with an active endoN (kindly provided by Karen Colley, University of Illinois, Chicago, IL) that specifically cleaves  $\alpha$ 2-8-linked polySia.<sup>27,28</sup> The following antibodies were used to stain monocytes, neutrophils, and macrophages: anti-CD45 (30-F11), anti-Ly6G (1A8), anti-CD11b (M1/70), anti-F4/80 (BM8), Siglec F (S17007L), anti-CD11c (HL3), and anti-CXCR-2 (SA044G4) (all from Biolegend, San Diego, CA), and anti-Ly6C (AL-21) from Becton Dickinson (Franklin Lakes, New Jersey). Following incubation at 4°C for 30 min with antibodies, cells were washed with PBS containing 2% human AB serum, fixed with 1% paraformaldehyde, acquired on a Guava easyCyte HT flow cytometer (Luminex, Austin, TX), and data were analyzed using FlowJo data analysis software (Tree Star, Ashland, OR).

### Adoptive transfer of WT and ST8SialV<sup>-/-</sup> leukocytes

Bone marrow monocytes and neutrophils from uninfected 8 to 12 week old WT and ST8SialV<sup>-/-</sup> mice were isolated as indicated above and adoptively transferred into recipient WT mice 24 h post-infection with *Spn*. Cells from ST8SialV<sup>-/-</sup> mice were labeled with CellTracker Deep Red Dye and the WT cells were labeled with Vybrant CFDA SE Cell Tracer Kit (both from Invitrogen, ThermoFisher Scientific) as per manufacturer's instructions. An equal number of WT and ST8SialV<sup>-/-</sup> monocytes or neutrophils was mixed together ( $2.5 \times 10^6$  cells of each type) in PBS and  $5.0 \times 10^6$  cells were injected intra-orbitally into infected WT recipient mice. Mice were sacrificed 24 h after cell transfer, organs were harvested and homogenized, and labeled donor cells in lung, spleen, peripheral blood and bone marrow were quantitated by flow cytometry.

### Cytokine measurement in lung homogenates

The amount of keratinocyte-derived chemoattractant CXCL-1/KC, IL-10, MCP-1 and IL-1 $\beta$  was determined in lung homogenates from *Spn*-infected WT and ST8SialV<sup>-/-</sup> mice by ELISA using mouse CXCL1/KC and MCP-1 Quantikine ELISA kits and mouse IL-1 $\beta$  and IL-10 DuoSet Elisa Kits (R&D Systems) following the manufacturer's protocol.

### Measurement of cell-bound cytokine and amount of total and phosphorylated ERK1/2

To determine binding of KC/CXCL-1 to neutrophils, BM neutrophils were enriched as above and  $4 \times 10^6$  cells in 0.20 mL RPMI/0.1% BSA were incubated for 30 min with CXCL-1 (100 ng/mL) at 37°C in 5% CO<sub>2</sub>. Cells were washed with 1 mL PBS, collected by centrifugation, resuspended in 1 mL PBS, transferred to a new tube and washed with an additional 1 mL of PBS. Cell pellets were lysed in radioimmune precipitation assay (RIPA) solution containing 50 mM Tris-HCl, pH 7.4, 100 mM NaCl, 0.5% Triton X-100, 0.5% sodium deoxycholate, 0.1% SDS, protease inhibitors (1:100 dilution of protease inhibitor cocktail; Sigma-Aldrich, St Louis, MO), 1 mM phenylmethylsulfonyl fluoride, 1 mM sodium fluoride, 1 mM sodium orthovanadate and 1 mM EDTA at 4°C for 30 min, the lysate was centrifuged at 10,000 x g for 10 min, and the amount of CXCL-1 in the supernatant was measured using a mouse CXCL1/KC Quantikine Elisa Kit. To measure the amount of total and phosphorylated ERK1/2 following cell activation, neutrophils were treated with 1  $\mu$ M fMLP for 2.5, 5, and 10 min, collected, lysed in RIPA buffer and analyzed by immunoblot as indicated below.

### Immunoblot analysis of cellular proteins

Cells were collected and solubilized for 30 min at 4°C in RIPA solution, and were centrifuged at 10,000 x g for 10 min at 4°C to remove insoluble material. Protein concentration in resultant supernatants was determined using a Bicinchoninic Acid/copper sulfate mix and indicated amounts of protein were resolved by electrophoresis on a 8% SDS-polyacrylamide gel using Tris-glycine-SDS running buffer (gel and running buffer from Invitrogen), electrotransferred by a semi-wet method to a Sequi-Blot PVDF membrane (Bio-Rad, Hercules, CA) and probed with 0.5  $\mu$ g/mL mouse mAb 735 against polySia (Absolute Antibody, Boston, MA), 0.2  $\mu$ g/mL rabbit Ab to phosphorylated ERK1/2 (clone 197G2; Cell Signaling Technology, Danvers, MA) or mouse Ab to total ERK1/2 (clone MK1; Santa Cruz Biotechnology, Santa Cruz, CA). The respective blots were incubated with 20 ng/mL of horseradish peroxidase-mouse IgG-BP (Santa Cruz Biotechnology) or with anti-rabbit IgG (R&D Systems), developed using an ECL chemiluminescence substrate kit (Amersham Biosciences, Piscataway, NJ) and read digitally on a ChemiDoc Imaging System (Bio-RAD, Hercules, CA). Immunoblots were quantified by densitometry using Molecular Analyst software (Bio-RAD). To reprobe PVDF membranes with a different Ab, previously bound Abs were stripped for 30 min at 50°C in a solution containing 62.5 mM Tris (pH 6.8), 100 mM b-mercaptoethanol, and 2% SDS.

### Phagocytosis assay of peritoneal and alveolar cells

Macrophages were harvested from the peritoneal cavity of WT and ST8SialV<sup>-/-</sup> mice 3 days after intraperitoneal injection with 3% thioglycolate.<sup>16</sup> Briefly,  $5 \times 10^5$  cells in RPMI/10% FCS were placed in culture for 24 h at 37°C in a CO<sub>2</sub> incubator in Corning Costar 24-well tissue culture plates. Prior to use, *Spn* was grown to mid-exponential phase in THB medium, collected by centrifugation (2700 x g, 10 min, 25°C) and incubated in RPMI/10% FCS containing 10% baby rabbit complement and 10% rabbit anti-strep antibody (both from BIORAD, Hercules, CA) for 30 min at 37°C. The macrophage monolayer was exposed to  $1 \times 10^8$  CFU of *Spn* (MOI of 200:1) in a final volume of 0.550 mL RPMI/10% FCS for 30 min at 37°C, incubated with medium containing penicillin to eliminate extracellular *Spn*, washed two times with PBS, lysed in 1 mL 1% Triton X-100 in PBS and plated on blood agar plates to quantitate the number of phagocytosed bacteria.<sup>16</sup> Alveolar leukocytes (predominantly macrophages) were harvested by BAL 20 h after I.T. instillation of LPS (25  $\mu$ g) using PBS (prewarmed to 37°C) containing 2 mM EDTA and 0.05% FCS and were treated with AKC lysis buffer to remove residual RBCs.  $6 \times 10^6$  leukocytes were incubated with  $1.2 \times 10^9$  CFU *Spn* (MOI of 200:1) prepared from the mid-exponential growth phase that were preincubated with baby rabbit complement and 10% anti-strep antibody as indicated above in a total volume of 0.5 mL RPMI/5% FCS. The cells were incubated for 4 h at 37°C in a 5% CO<sub>2</sub> incubator, were washed 3 times with 25 X volume PBS and were processed as above for plating on blood agar plates to quantitate the number of phagocytosed bacteria.

**Microfluidic-based microchannel cell migration assay** Microfluidic devices consisting of an array of parallel microchannels of prescribed length ( $L = 200 \mu\text{m}$ ), height ( $H = 3 \mu\text{m}$ ) and width ( $W = 3 \mu\text{m}$ ) were fabricated from polydimethylsiloxane (PDMS) using photolithography and a standard replica molding technique.<sup>51–53</sup> Channels were coated with 20  $\mu$ g/mL collagen (Gibco, ThermoFisher Scientific) to facilitate binding of neutrophils. Cells were harvested from the BM of WT and ST8SialV<sup>-/-</sup> mice, and neutrophils were enriched to greater than 80% purity by histopaque gradient centrifugation as described above. Enriched neutrophils were resuspended at  $1\text{--}3 \times 10^7$  cells/ml in RPMI 1640 medium containing 0.1% BSA (Millipore Sigma, MA) and 20  $\mu$ L of cell suspension (equivalent to  $2\text{--}6 \times 10^5$  cells) was added to the seeding channel inlet to create a pressure-driven flow of cells across the seeding region. Once cells reached the outlet, the flow was arrested by transferring 10  $\mu$ L of cell suspension to the opposite side. Cells were allowed to adhere for 10 min. Media in the inlet wells was then removed and replaced with fresh RPMI 1640/0.1% BSA. A chemoattractant gradient of fMLP (starting with upper concentration of 87.5  $\mu$ g/mL or 200  $\mu$ M; Sigma-Aldrich) or CXCL1 (10  $\mu$ g/mL or 900 nM; R&D Systems) in RPMI 1640/0.1% BSA was established by adding media to the top wells in the cell exit region. Migration of neutrophils into the microchannels was visualized and recorded with live-cell time-lapse microscopy in an enclosed and humidified microscope stage maintained at 37°C with 5% CO<sub>2</sub> (Tokai-Hit, Shizuoka-hen, Japan). Phase-contrast images were taken every 1 min for a total duration of 35 min with a 20x/0.45 NA Ph1 objective on a Nikon Eclipse Ti inverted microscope (Nikon, Tokyo, Japan). Cells were

analyzed using the MTrackJ plugin in ImageJ (National Institutes of Health, Bethesda, MD). The speed (defined as the average distance traveled between each time interval), velocity (defined as the net cell displacement over total migration time), and persistence (defined as the ratio of net cell displacement over total migration path) of each cell was computed from individual cell tracks.

### Transwell cell migration assay

Quantitative transwell migration assays for WT and ST8SialV<sup>-/-</sup> BM neutrophils and monocytes were performed using QCM chemotaxis 96-well migration kits (EMD Millipore, Burlington, MA) with 5  $\mu$ m pore sizes. As per the manufacturer's instructions,  $2 \times 10^4$  neutrophils or  $1 \times 10^5$  monocytes in 100  $\mu$ L RPMI/0.1% BSA was placed in the top chamber of the well with the lower chamber containing 150  $\mu$ L of RPMI/0.1% BSA with or without 100 ng/mL chemokine CXCL-1 (R&D Systems) or CCL2 (GeminiBio, Sacramento, CA), respectively. After a 1 h (neutrophils) or 24 h (monocytes) incubation at 37°C in 5% CO<sub>2</sub>, cells that migrated into the lower chamber or remained attached to the bottom of the filter were collected, lysed, and stained with fluorescent dye CyQuant GR and fluorescence was quantified on a SpectraMax iD3 Multi-Mode Microplate Reader with a 480/520 nm filter set (Molecular Devices, San Jose, CA). All assays were performed in triplicate. A standard curve for fluorescence and number of cells was established for each experiment to calculate migrated cell count.

### Intravital microscopy of cremasteric microcirculation

Mice were anesthetized with an intraperitoneal injection of 100 mg/kg Ketamine and 10 mg/kg Xylazine, placed supine on a heated surgery/microscope stage with legs straddling the pedestal, and secured in position with tape loosely placed across the chest and both legs. After the testicular area, legs and lower abdomen were shaved and the bladder emptied with gentle pressure, the testicles were lowered by gentle pressure on the abdomen, and the cremasteric muscle was surgically separated from surrounding tissue and pinned to the pedestal. An incision extending along a line drawn by the prolongation of the femoral artery and the iliac vein to the base of the testicle allowed the epididymis and testes to be visualized and separated from the cremaster muscle which was immediately perfused continuously with warmed PBS (37°C) at a rate of 1 mL/min. Two hours prior to cremaster muscle exposure, mice were placed under light isoflurane anesthesia and were injected intrascrotally with 500 ng murine TNF $\alpha$  (R&D Systems), to induce inflammation. An equal number of BM neutrophils from WT (labeled with Vybrant CFDA SE) or ST8SialV<sup>-/-</sup> mice (labeled with CellTracker Deep Red Dye) were mixed together in HBSS at  $10^8$  cells/ml and  $2.0 \times 10^7$  cells were injected (200  $\mu$ L per mouse) retro-orbitally into recipient WT mice. Blood vasculature was visualized by injecting 50  $\mu$ L of Dextran Texas Red 70, 2 mg/ml (Invitrogen) intravenously. Rolling, adhesion, and velocity of labeled cells were recorded for 2–3 min in 3–5 venules from each mouse using a Zeiss 710 non-linear optical (NLO) microscope with Plan-Apochromat<sup>®</sup> 10x/0.45 M27 non immersion objective (Carl Zeiss). To evaluate neutrophil extravasation, blood vessels of recipient mice with a diameter of 20–45  $\mu$ m were observed for 0.5–2 h using an upright Zeiss Neo 710 confocal laser scanning microscope and a 10 $\times$ -air objective (NA 1.0). The number of extravasated donor WT and ST8SialV<sup>-/-</sup> neutrophils per field were manually counted. Data were analyzed by tracking individual neutrophils using Imaris software (Bitplane).

### Apoptosis assay

Alveolar leukocytes were harvested by BAL as described above and stained with antibodies against CD45, CD11c, SiglecF and with Annexin V and 7-AAD from an Apoptosis Detection Kit (Becton Dickinson Biosciences, Franklin Lakes, NJ) as per manufacturer's directions. The percentage of alveolar macrophages displaying early apoptosis was analyzed by flow cytometry.

## QUANTIFICATION AND STATISTICAL ANALYSIS

All experimental data were analyzed using Prism software (GraphPad) with two-tailed unpaired Student's t-test, log rank test, Welch's t test, non-parametric Wilcoxon signed-rank test and with one way ANOVA tests. All experiments were repeated at least three times and are presented as the mean  $\pm$  SEM or SD. \* $p \leq 0.05$ , \*\* $p \leq 0.01$ , \*\*\* $p \leq 0.001$ .